Title

Tris(carbene)borates; alternatives to cyclopentadienyls in organolanthanide chemistry

Journal

Dalton Transactions, 52(17)

ISSN

1477-9226

Authors

Price, Amy N

Gupta, Ankur K

de Jong, Wibe A

et al.

Publication Date

2023-05-02

DOI

10.1039/d3dt00718a

ChemComm

Tris(carbene)borates; a new alternative for cyclopentadienide in organolanthanide chemistry

Journal:	*ChemComm*
Manuscript ID	Draft
Article Type:	Communication

Tris(carbene)borates; New alternatives to cyclopentadienyls in organolanthanide chemistry

Received 00th January 20xx,
Accepted 00th January 20xx

DOI: 10.1039/x0xx00000x

Amy N. Price,[a,b] Ankur Gupta,[c] Wibe de Jong,[c] Polly Arnold[a,b]*

The chemistry of the tris-carbene anion phenyltris(3-alkyl-imidazoline-2-yliden-1-yl)borate, **[C3^{Me}]$^-$** ligand, is initiated in the f-block. Neutral molecular complexes of the form **Ln(C3)$_2$I** are formed for cerium(III), while a solvent-separated ion pair **[Ln(C3)$_2$]I** forms for ytterbium(III). DFT/QTAIM computational analysis of the complexes and related tridentate tris(pyrazolyl)borate (**Tp**) supported analogs demonstrates the anticipated strength of the σ donation and confirms greater covalency in the metal-carbon bonds of the **[C3^{Me}]$^-$** complexes in comparison with those in the **Tp^{Me,Me}** complexes. The DFT calculations demonstrate the crucial role of THF solvent in accurately reproducing the contrasting molecule and ion-pair geometries observed experimentally for the Ce and Yb complexes.

Introduction

There are still relatively few ligands in f-block chemistry organometallic chemistry that bind to the f-block metal cations using only carbon atoms, despite the field now being more than fifty years old. Cyclopentadienyl ligands, monoanionic, six-electron donors $[C_5H_nR_{5-n}]^-$ (n = 1-5) have dominated the field,[1] with the cyclic dianionic ligand cyclooctadienide (COT^{2-}) close behind,[2-6] but few other competitors, e.g. cyclobutadienide .[7-11] Lanthanide organometallic complexes have demonstrated exciting properties, from single-molecule magnetism[12, 13] and molecular qubit behavior [14 15] to reductive activation of small molecules[16] and photocatalytic properties.[17, 18] New robust, monoanionic, and sterically bulky alternatives to these cyclic ligand sets should further expand the capabilities of molecular f-block compounds.

N-heterocyclic carbenes (NHCs) have seen application as σ-donating ligands to metals across the periodic table, and are highly tunable.[19-22] Yet ligands which coordinate through multiple carbenes have only rarely been used to bind f-block cations.[23-25] We recently reported, in collaboration with the Jenkins group, the use of macrocyclic tetradentate, dianionic tetracarbenes **[^{BMe2,Me}TC^{H}]$^-$** in Fig. 1, to form homoleptic thorium (IV) and uranium (IV) carbene 'sandwich' complexes.[26]

Neutral, homoleptic bis(NHC)borate complexes have been made for a few rare earth trications (Y, Tb, Dy, Ho, Er), and the ligand field that they imparted on the Tb and Dy ions shown to generate single-molecule magnet (SMM) behavior with a magnetization relaxation that is orders of magnitude slower than in the isomeric bis(pyrazolyl)borate analogues.[27]

We considered that the monoanionic, phenyltris(3-alkyl-imidazoline-2-yliden-1-yl)borate **[C3^{R}]$^-$** in Fig. 1, which has been used extensively to support first-row transition metal complexes with unusual electronic structures, [28-31] could support unusual new f-block chemistry.[32, 33] It is isolobal to Cp^- and the tris(pyrazolyl)borate ligand **[Tp$^{R,R'}$]$^-$** in Fig. 1, an N_3-donor that has a long history in f-block chemistry, even though it is susceptible to B-N cleavage, and is not oxidatively stable.[34, 35]

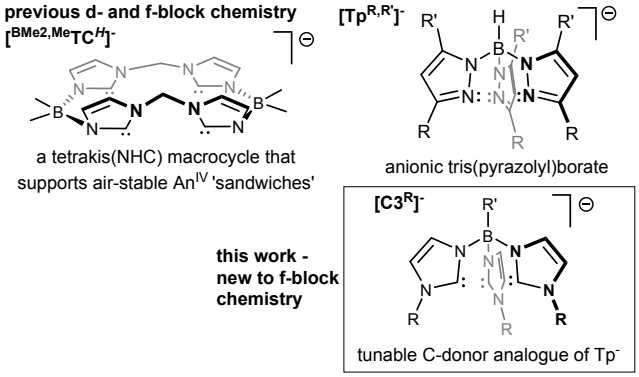

Figure 1. Multidentate ligands with anionic borate backbones as potential replacements for carbocyclic anions such as cyclopentadienyl, Cp^-.

Here, we report **C3** complexes of Ce^{III} and Yb^{III}, representing the beginning and end of the series, and a DFT/QTAIM computational analysis of their electronic structures. Topological analyses of the metal complexes using the QTAIM[36] theory have helped us further understand and quantify the covalent nature of the metal-ligand bonds. The QTAIM metrics, the ratio of Lagrangian kinetic energy and potential energy density at the bond critical point (BCP) (commonly represented as $\frac{-G_{BCP}}{V_{BCP}}$ symbolically) and the delocalization index ($\delta(\mathbf{M},\mathbf{X})$) have been found to be effective in identifying covalency trends in actinide complexes.[37, 38] Therefore, we have applied these metrics in the present work to broaden their applicability.

Results and Discussion

The cerium complex **Ce(C3)$_2$I** can be obtained from the reaction of two equivalents of **Li[C3]** and $CeI_3(thf)_4$ at room temperature, Scheme 1. **Ce(C3)$_2$I** was found to be stable in thf at 70°C for up to 80 hours with only minor degradation, while the tris(pyrazolyl)borate analog **Ce(Tp*)$_2$I** was reported to be unisolable,[39] although it could be made *in situ* and converted to

[a] *Chemical Sciences Division, Lawrence Berkeley National Laboratory Berkeley, CA 94720, USA*
[b] *Department of Chemistry, University of California, Berkeley Berkeley, CA 94720-1460, USA.*
[c] *Computer Sciences Division, Lawrence Berkeley National Laboratory Berkeley, CA 94720, USA*

Electronic Supplementary Information (ESI) available: [Additional information about synthesis, crystallography and calculations, Crystal structure cifs deposited in the CSD (2235950-2235953)]. See DOI: 10.1039/x0xx00000x

the stable bipyridyl adduct **Ce(Tp*)$_2$(bipy)**, which contains a formally mono-reduced bipy$^{\cdot-}$ radical anion. To enable comparisons of the chelate ligands, we made **Ce(C3)$_2$(bipy)** from the reaction between **Ce(C3)$_2$I** and K[bipy] in THF.

Ytterbium(III) is significantly smaller than Ce(III) ($r_{cov,\ 6\text{-coord}}$ Ce^{III} = 1.15; Yb^{III} = 1.008 Å)[40]. The reaction of $YbI_3(thf)_{1.5}$ with two equivalents of **Li[C3]** results in the formation of a solvent separated ion pair **[Yb(C3)$_2$]I**, with two [**C3**]$^-$ ligands coordinated to the ytterbium center, and an outer-sphere iodide. This is analogous to the solvent separated ion pair [Yb(Tp*)$_2$]OTf.[41]

Once made, **[Yb(C3)$_2$]I** is insoluble in THF, unlike molecular **Ce(C3)$_2$I** which is highly THF-soluble. The mono(**C3**) complex **Li[Ce(C3)I$_3$]** can also be made from the equimolar reaction between $CeI_3(thf)_4$ and **Li[C3]** (see SI for details and the solid state structure). Addition of a second equivalent of **Li[C3]** to **Li[Ce(C3)I$_3$]** swiftly gives **Ce(C3)$_2$I**, observed via ^{1}H-NMR spectroscopy, although addition of further $CeI_3(thf)_4$, quickly regenerates **Li[Ce(C3)I$_3$]**, Scheme 1, demonstrating that the [**C3**] NHC chelate binds Ce^{III} more strongly than Li^I but that these monoanions can exchange rapidly. The solid-state structures of the three bis(**C3**) complexes (Figure 1) are discussed below along with the computation results arising from DFT geometry optimizations and electronic structure calculations (Table 1 above, further details are included in the SI).

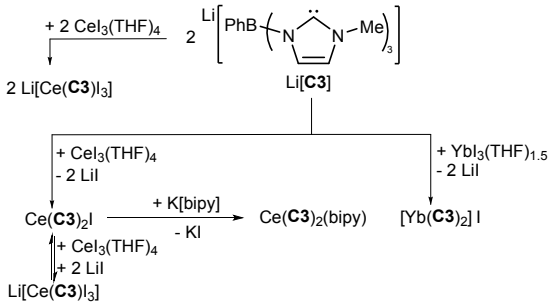

Scheme 1: Ce and Yb complexes of [**C3**]$^-$ can be prepared from Li[**C3**]$^-$ and the respective $LnI_3(thf)_n$ salt via salt metathesis.

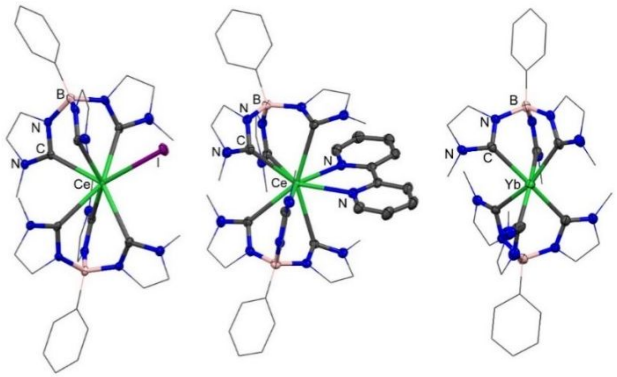

Figure 2. Solid-state structures of a) **Ce(C3)$_2$I**, b) **Ce(C3)$_2$(bipy)**, and c) the cation of **[Yb(C3)$_2$]I**. peripheral carbons drawn as wireframe, hydrogen atoms, lattice solvent, and iodide counterion in c) omitted for clarity. C= grey, Ce, Yb= green, N=blue B=pink, I=purple.

Table 1. QTAIM metrics for the metal-ligand bonds in the optimized lanthanide borate complexes. **BCP** = Bond critical point, $\boldsymbol{\rho_{BCP}}$ = Electron density at BCP, $\nabla^2\boldsymbol{\rho_{BCP}}$ = Laplacian of the electron density at BCP, $\boldsymbol{G_{BCP}}$ = Lagrangian kinetic energy, $\boldsymbol{V_{BCP}}$ = Potential energy density, $\boldsymbol{\delta(M,X)}$ = Delocalization Index

Metal Complex	Bond Length (Å)	$\boldsymbol{\rho_{BCP}}$	$\nabla^2\boldsymbol{\rho_{BCP}}$	$\frac{-G_{BCP}}{V_{BCP}}$ (Mean)	$\boldsymbol{\delta(M,X)}$ (Mean)
Ce(C3)$_2$I	2.63 – 2.84	0.034 – 0.053	0.063 – 0.083	0.767 – 0.855 (0.801)	0.253 – 0.346 (0.306)
[Yb(C3)$_2$]I	2.43 – 2.50	0.052 – 0.060	0.122 – 0.142	0.803 – 0.820 (0.811)	0.288 – 0.326 (0.304)
Ce(C3)$_2$ (bipy)	2.70 – 2.82	0.032 – 0.045	0.062 – 0.080	0.810 – 0.873 (0.832)	0.216 – 0.302 (0.270)
Ce(Tp*)$_2$ (bipy)	2.57 – 2.71	0.036 – 0.049	0.095 – 0.124	0.864 – 0.921 (0.893)	0.212 – 0.275 (0.239)
[Yb(Tp*)$_2$]I	2.31 – 2.35	0.061 – 0.066	0.201 – 0.216	0.854 – 0.866 (0.861)	0.287 – 0.314 (0.296)

The structures of **Ce(C3)$_2$I** and **Ce(C3)$_2$(bipy)** are similar, with a B-Ce-B angle of 144.64(5)° in **Ce(C3)$_2$I** and 144.64(5)° in **Ce(C3)$_2$I**. The Ce-C range is 2.631(2) - 2.781(2) Å in **Ce(C3)$_2$I**, slightly shorter than in **Ce(C3)$_2$(bipy)** (2.7016(17) to 2.8270(17) Å), likely due to reduced steric hindrance about cerium in the former. (Median Ce(III) carbene distance in CCDC = 2.749 Å.) The computed Ce-C bonds agree with experiment, and are in line with greater covalency of the Ce-C bonds in **Ce(C3)$_2$I**.

The $\frac{-G_{BCP}}{V_{BCP}}$ ratio is typically between 0.5 and 1.0 for covalent bonds, with a lower value indicating a higher degree of covalency; while $\boldsymbol{\delta(M,X)}$ represents the approximate number of electron pairs shared between two atomic basins; a higher $\boldsymbol{\delta(M,X)}$ value for a bond signifies a higher level of covalency. Calculated values of $\boldsymbol{\rho_{BCP}}$ and $\nabla^2\boldsymbol{\rho_{BCP}}$ for the Ce-C bonds indicate that the Ce-C bonding is primarily ionic, while $\frac{-G_{BCP}}{V_{BCP}}$ is calculated to range between 0.767-0.855 for **Ce(C3)$_2$I** and 0.810-0.873 for **Ce(C3)$_2$(bipy)**, suggesting slightly more covalent Ce-C bonding for **Ce(C3)$_2$I** than **Ce(C3)$_2$(bipy)**. The Yb-C distances in **[Yb(C3)$_2$]I** range between 2.379(5)- 2.481(4) Å, and the B-Yb-B angle is 155.3(1)°. The distortion from pseudo-octahedral geometry around the Yb(III) center is in contrast to that observed in the reported Tp* analogue, which has a crystallographically enforced B-Yb-B angle of 180°.

A similar and small amount of covalency in the Ln-C bonds was found for **Ce(C3)$_2$I** and **[Yb(C3)$_2$]I** using QTAIM analysis: $\frac{-G_{BCP}}{V_{BCP}}$ for the Yb-C bonds in **[Yb(C3)$_2$]I** (between 0.803 and 0.820) were similar to the values for **Ce(C3)$_2$I**, although in a narrower range, reflecting the narrower range of M-C distances in **[Yb(C3)$_2$]I** compared to **Ce(C3)$_2$I** (a result of greater symmetry).

It is instructive to compare the physical and electronic structures of **Ce(C3)$_2$(bipy)** with **Ce(Tp*)$_2$(bipy)**.[39] The SI contains an analysis of the steric similarity of **C3** and **Tp***.

Structurally, **Ce(C3)$_2$(bipy)** and **Ce(Tp*)$_2$(bipy)** are very similar, with B-Ce-B angles of 145.05(4) and 146.7(1)° respectively, while the Ce-N_{bipy} distances in **Ce(C3)$_2$(bipy)** are slightly longer than in **Ce(Tp*)$_2$(bipy)** (2.612(4) v.s. 2.592(4) Å) potentially due to more electron density on the cerium(III) center in **Ce(C3)$_2$(bipy)**, as a result of strong σ-donation from the tris(carbene) ligands.

The partial atomic charges for all the metal complexes were computed using the QTAIM and NPA schemes, Table S1 in the SI. As is normal, the metal atom charges are lower than their formal oxidation state of +3 in all cases due to ligand-to-metal electron (charge) transfer, which appears greatest for each **C3** adduct.

Analysis of $\boldsymbol{\rho_{BCP}}$ (electron density at BCP) and $\boldsymbol{\nabla^2\rho_{BCP}}$ (Laplacian of the electron density at BCP) suggest that the bonding for both the Ce-C bonds in **Ce(C3)$_2$(bipy)** and the Ce-N_{Tp*} bonds in **Ce(Tp*)$_2$(bipy)** are primarily ionic in nature. However, the slightly lower value of $\frac{-G_{BCP}}{V_{BCP}}$ at BCPs for the Ce-C bonds (0.810-0.873) in **Ce(C3)$_2$(bipy)** compared to the Ce- N_{Tp*} bonds in **Ce(Tp*)$_2$(bipy)** (0.874-0.921 Å), suggests slightly more covalent character for the Ce-C bonds in **Ce(C3)$_2$(bipy)**.

The calculations show that the frontier orbital energies for the Tp* complexes are slightly lower than those of their [**C3**] counterparts, for both the Ce bipy complexes and the Yb complexes (Figure 3 for Yb and Figure S5 for Ce in the SI). The SOMO-LUMO gaps for the bipy complexes are close in energy at 1.58 eV and 1.56 eV for **Ce(C3)$_2$(bipy)** and **Ce(Tp*)$_2$(bipy)**, while the SOMO LUMO gaps for **[Yb(C3)$_2$]I** and **[Yb(Tp*)$_2$]I** are 3.99 and 3.14 eV respectively (ignoring the electrons in the HOMO to HOMO-2 orbitals which are on the I^- counterion), suggesting greater oxidative stability for **[Yb(C3)$_2$]I**. Both bipy complexes exist in the triplet spin state with one electron on Ce and one on the bipy radical with unpaired electrons on the Ce center and the bipyridyl ligand. The UV-Vis absorption spectra of **Ce(C3)$_2$I** and **Ce(C3)$_2$bipy** were calculated using the time-dependent density functional theory (TD-DFT) method and were compared with the experimental spectra, with the computed spectra validating the theoretical predictions (Figures S1 and S3 in the SI, further details about these calculations and the frontier orbitals for the Ce complexes are also in the SI).

The bonding is surprisingly different in the two Yb complexes: first, the LUMO in **[Yb(C3)$_2$]I** is f_{z^3} ($m_l = 0$, σ anti-bonding) while in **[Yb(Tp*)$_2$]I** it is computed to be f_{xyz} ($m_l = +2$, δ anti-bonding). Further, and in contrast with the Ce complexes, the unpaired spin in the 4f orbital of the Yb atom is confined within lower energy occupied molecular orbitals, rather than those near the HOMO. Comparing the two Yb complexes, the 4f orbitals of **[Yb(Tp*)$_2$]I** are more hybridized than those of **[Yb(C3)$_2$]I**, as indicated by the lower number of molecular orbitals with over 90% f-orbital contribution (only 3 in **[Yb(Tp*)$_2$]I** vs. 7 in **[Yb(C3)$_2$]I**). These data suggest the two different ligands can generate different preferred f-orbital use by the Ln center.

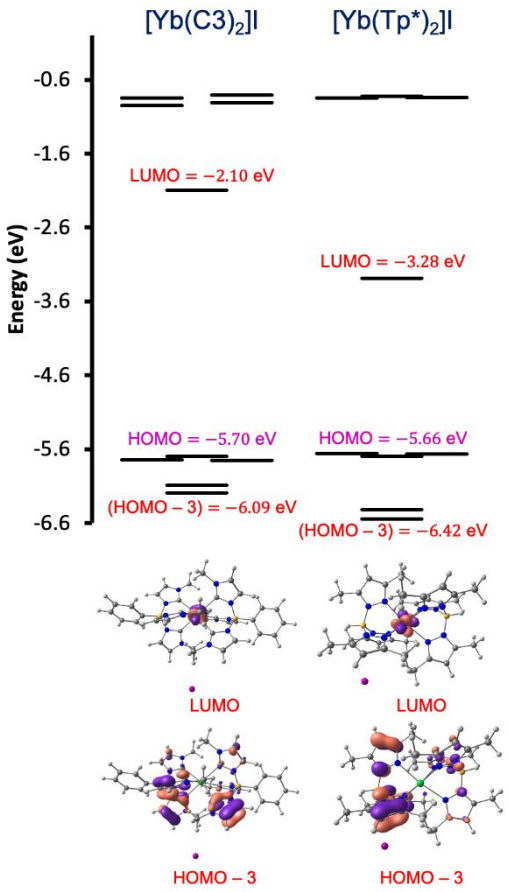

Figure 3. Calculated frontier molecular orbital diagrams for the Yb borate complexes. The three nearly degenerate HOMOs for the Yb complexes (shown in magenta) are exclusively localized on the non-bonded iodine ion.

In conclusion, the coordination chemistry of tris(NHC) borates has been extended to the lanthanides cerium and ytterbium. Neutral molecular complexes of the form **Ln(C3)$_2$I** are favored for the larger cerium ion, while a solvent-separated ion pair of the form **[Ln(C3)$_2$]I** forms for ytterbium, resulting in dramatically different solubilities of the resulting complexes. We suggest that this may have potential use in the separation of lanthanide ions. Calculated QTAIM metrics, including $\frac{-G_{BCP}}{V_{BCP}}$ suggest that the tris(carbene) borate ligands form slightly more covalent bonds with cerium and ytterbium than the N-donor tris(pyrazolyl)borates, and greater covalency calculated for the Ce-C bonds in **Ce(C3)$_2$I** than the bipyridyl adduct **Ce(C3)$_2$(bipy)**. Future work will study the use of these ligands to isolate specific rare earth ions and an investigation of their photophysical properties.

Conflicts of interest

The authors declare no conflicts of interest

Acknowledgements

The project was funded by the U.S. Department of Energy (DOE), Office of Science, Office of Basic Energy Sciences, Chemical Sciences, Geosciences, and Biosciences Division, in the Heavy Element Program (some synthetic efforts), the Molecular f-element qubits project (Yb complex analyses) and the Rare Earth Project in the Separations Program (remainder), at the Lawrence Berkeley National Laboratory under Contract DE-AC02-05CH11231. We acknowledge Hasan Celik for NMR support and the (NIH) for funding the NMR facility under grant nos. SRR023679A, S10OD024998 and 1S10RR016634-01.

References

1. R. A. Kresinski, in *Encyclopedia of Inorganic and Bioinorganic Chemistry*, DOI: https://doi.org/10.1002/9781119951438.eibc2032.
2. F. Mares, K. Hodgson and A. Streitwieser, *J. Organomet. Chem.*, 1970, **24**, C68-C70.
3. F. Mares, K. O. Hodgson and A. Streitwieser, *J. Organomet. Chem.*, 1971, **28**, C24-C26.
4. J. D. Jamerson, A. P. Masino and J. Takats, *J. Organomet. Chem.*, 1974, **65**, C33-C36.
5. J. Rausch, C. Apostolidis, O. Walter, V. Lorenz, C. G. Hrib, L. Hilfert, M. Kühling, S. Busse and F. T. Edelmann, *New J. Chem.*, 2015, **39**, 7656-7666.
6. A. Greco, S. Cesca and W. Bertolini, *J. Organomet. Chem.*, 1976, **113**, 321-330.
7. J. P. Durrant, B. M. Day, J. Tang, A. Mansikkamäki and R. A. Layfield, *Angew. Chem. Int. Ed.*, 2022, **61**.
8. N. Tsoureas, A. Mansikkamaki and R. A. Layfield, *Chem. Commun.*, 2020, **56**, 944-947.
9. N. Tsoureas, A. Mansikkamäki and R. A. Layfield, *Chem. Sci.*, 2021, **12**, 2948-2954.
10. J. T. Boronski, L. R. Doyle, J. A. Seed, A. J. Wooles and S. T. Liddle, *Angew. Chem. Int. Ed.*, 2020, **59**, 295-299.
11. J. T. Boronski and S. T. Liddle, *Eur. J. Inorg. Chem.*, 2020, **2020**, 2851-2861.
12. R. A. Layfield, *Organometallics*, 2014, **33**, 1084-1099.
13. M. J. Heras Ojea, L. C. H. Maddock and R. A. Layfield, Springer International Publishing, 2019, DOI: 10.1007/3418_2019_26, pp. 253-280.
14. E. Moreno-Pineda and W. Wernsdorfer, *Nature Reviews Physics*, 2021, **3**, 645-659.
15. K. Kundu, J. R. K. White, S. A. Moehring, J. M. Yu, J. W. Ziller, F. Furche, W. J. Evans and S. Hill, *Nature Chemistry*, 2022, **14**, 392-397.
16. Y. Yao and Q. Shen, in *Rare Earth Coordination Chemistry*, 2010, DOI: https://doi.org/10.1002/9780470824870.ch8, pp. 309-353.
17. P. L. Watson, T. H. Tulip and I. Williams, *Organometallics*, 1990, **9**, 1999-2009.
18. A. E. Kynman, L. K. Elghanayan, A. N. Desnoyer, Y. Yang, L. Sévery, A. Di Giuseppe, T. D. Tilley, L. Maron and P. L. Arnold, *Chem. Sci.*, 2022, **13**, 14090-14100.
19. M. Poyatos, J. A. Mata and E. Peris, *Chem. Rev.*, 2009, **109**, 3677-3707.
20. P. L. Arnold and I. J. Casely, *Chemical Reviews*, 2009, **109**, 3599-3611.
21. M. Jalal, B. Hammouti, R. Touzani, A. Aouniti and I. Ozdemir, *Mater Today Proc*, 2020, **31**, S122-s129.
22. L. Zapf, U. Radius and M. Finze, *Angew. Chem. Int. Ed.*, 2021, **60**, 17974-17980.
23. I. S. Edworthy, A. J. Blake, C. Wilson and P. L. Arnold, *Organometallics*, 2007, **26**, 3684-3689.
24. M. E. Garner, S. Hohloch, L. Maron and J. Arnold, *Organometallics*, 2016, **35**, 2915-2922.
25. X. B. Carroll, D. Errulat, M. Murugesu and D. M. Jenkins, *Inorg. Chem.*, 2022, **61**, 1611-1619.
26. J. F. DeJesus, R. W. F. Kerr, D. A. Penchoff, X. B. Carroll, C. C. Peterson, P. L. Arnold and D. M. Jenkins, *Chem. Sci.*, 2021, **12**, 7882-7887.
27. K. R. Meihaus, S. G. Minasian, W. W. Lukens, Jr., S. A. Kozimor, D. K. Shuh, T. Tyliszczak and J. R. Long, *Journal of the American Chemical Society*, 2014, **136**, 6056-6068.
28. R. Fränkel, U. Kernbach, M. Bakola-Christianopoulou, U. Plaia, M. Suter, W. Ponikwar, H. Nöth, C. Moinet and W. P. Fehlhammer, *J. Organomet. Chem.*, 2001, **617-618**, 530-545.
29. J. A. Valdez-Moreira, D. M. Beagan, H. Yang, J. Telser, B. M. Hoffman, M. Pink, V. Carta and J. M. Smith, *ACS Cent Sci*, 2021, **7**, 1751-1755.
30. T. Nishiura, A. Takabatake, M. Okutsu, J. Nakazawa and S. Hikichi, *Dalton Transactions*, 2019, **48**, 2564-2568.
31. S. B. Muñoz, III, W. K. Foster, H.-J. Lin, C. G. Margarit, D. A. Dickie and J. M. Smith, *Inorg. Chem.*, 2012, **51**, 12660-12668.
32. M. Elie, J. L. Renaud and S. Gaillard, *Polyhedron*, 2018, **140**, 158-168.
33. L. Wang, Z. Zhao, G. Zhan, H. Fang, H. Yang, T. Huang, Y. Zhang, N. Jiang, L. Duan, Z. Liu, Z. Bian, Z. Lu and C. Huang, *Light: Science & Applications*, 2020, **9**, 157.
34. C. Apostolidis, A. Kovács, A. Morgenstern, J. Rebizant and O. Walter, *Inorganics*, 2021, **9**, 44.
35. P. L. Arnold, M. S. Sanford and S. M. Pearson, *Journal of the American Chemical Society*, 2009, **131**, 13912-13913.
36. R. F. W. Bader, *Acc. Chem. Res.*, 1985, **18**, 9-15.
37. V. E. J. Berryman, J. J. Shephard, T. Ochiai, A. N. Price, P. L. Arnold, S. Parsons and N. Kaltsoyannis, *Phys. Chem. Chem. Phys.*, 2020, **22**, 16804-16812.
38. V. E. J. Berryman, Z. J. Whalley, J. J. Shephard, T. Ochiai, A. N. Price, P. L. Arnold, S. Parsons and N. Kaltsoyannis, *Dalton Transactions*, 2019, **48**, 2939-2947.
39. F. Ortu, H. Zhu, M.-E. Boulon and D. P. Mills, *Inorganics*, 2015, **3**, 534-553.
40. R. Shannon, *Acta Crystallogr., Sect. A:*, 1976, **32**, 751-767.
41. G. H. Maunder, A. Sella and D. A. Tocher, *J. Chem. Soc., Chem. Commun.*, 1994, DOI: 10.1039/C39940000885, 885-886.

Supporting Information: Tris(carbene)borates; New alternatives to cyclopentadienyls in organolanthanide chemistry

Amy Price,[a,b] Ankur Gupta,[c] Wibe de Jong,[c] Polly Arnold[a,b]

[a]Chemical Sciences Division, Lawrence Berkeley National Laboratory, Berkeley, CA 94720, USA

[b]Department of Chemistry, University of California, Berkeley, Berkeley, CA 94720-1460, USA

[c]Computer Sciences Division, Lawrence Berkeley National Laboratory, Berkeley, CA 94720, USA

Table of Contents

	Page
General information	**2**
Synthesis and characterization	**2**
SAMBVCA 2.1 Analysis of Tp* vs. C3	**9**
Crystallographic details	**14**
Computational details	**17**
References	**31**

General information

All moisture and air sensitive materials were manipulated using standard high-vacuum Schlenk-line techniques and MBraun gloveboxes and stored under an atmosphere of dried and deoxygenated argon. All glassware items, cannulae and Fisherbrand 1.2 µm retention glass microfibre filters were dried in a 160 °C oven overnight before use. Hexanes, tetrahydrofuran (THF), diethyl ether (Et_2O) and toluene for use with moisture and air sensitive compounds were dried using an MBRAUN SPS 800 Manual solvent purification system and stored over activated 3 Å molecular sieves. Benzene-d6 was purchased from Cambridge Isotope Laboratories and were refluxed over potassium metal for 24 hours, freeze-pump-thaw degassed and purified by trap-to-trap distillation prior to use. THF-d8 was purchased from Cambridge Isotope Laboratories and dried over sodium/benzophenone before being freeze-pump-thaw degassed and purified by trap-to-trap distillation prior to use. Methylene dichloride-d2 was purchased from Cambridge Isotope Laboratories and dried over calcium hydride and purified by trap-to-trap distillation before use. All solvents were purchased from Sigma-Aldrich or Fisher Scientific and stored over 3 Å molecular sieves for 4 hours before being used. $CeI_3(thf)_4$, $YbI_3(thf)_{1.5}$, lithium diisopropyl amide, KC_8 and phenylborontrimethylimidazolium ditriflate ([**C3**H_3].2[OTf]) were prepared according to literature methods.[1-4] All other chemicals were purchased from commercial suppliers and degassed and/or dried under vacuum or over 3 Å molecular sieves for 12 hours before use. NMR spectra were recorded on Bruker Avance 400 or 500 MHz spectrometers and are referenced to residual protio solvent (3.58 and 1.72 ppm for THF-d_8, 7.16 ppm for benzene-d_6, 5.32 for dichloromethane-d_2) for 1H NMR spectroscopy. Chemical shifts are quoted in ppm. NMR spectra were measured at 25°C unless otherwise noted. Elemental analyses were carried out by the microanalytic services in the College of Chemistry at the University of California, Berkeley. 10 mm pathlength quartz cells with Teflon lined screw caps were used for collecting photophysical data of all air sensitive compounds: the samples were prepared under an argon atmosphere for electronic absorption spectra (UV-Vis). UV-Vis measurements were collected on an Agilent Varian Cary 50 UV-Vis spectrophotometer. Single crystal X-ray diffraction data of all other compounds were collected using a Rigaku Xtalab Synergy-S diffractometer fitted with a HyPix-6000HE photon counting detector using MoKα (λ = 0.71073 Å) or CuKα (λ = 0.1.5418Å) radiation. All structures were solved using SHELXT in Olex2 and refined using SHELXL in Olex2.13.[5, 6] Absorption corrections were completed using CrysAlis PRO (Rigaku Oxford Diffraction) software. Analytical numeric absorption corrections used a multifaceted crystal model based on expressions derived by Clark and Reid.[7] Numerical absorption correction was based on a Gaussian integration over a multifaceted crystal model.

Synthetic Methods and Characterisation

Li[C3]

Prepared via a minor modification of a previously reported method.[8] To a stirred suspension of phenylborontrimethylimidazolium ditriflate ([**C3**H_3].2[OTf]) (1.0 g, 1.75 mMol) in diethyl ether, 10 mL, was added 3.3 equivalents of lithium diisopropyl amide (0.62 g, 5.8 mMol) with stirring. The suspension was stirred for 2 hours until the supernatant liquors were yellow/brown and a fine powdery pale tan precipitate formed. The mixture was left to stand at -35°C overnight, then the supernatant was removed by decantation. The remaining pale tan precipitate was washed once with diethyl ether (5 mL) and twice with hexane (5 mL); each time after allowing the precipitate to settle by storage at -35°C for at least one

hour. The precipitate was dried under vacuum to yield **Li[C3]** as a white to tan powder (0.52 g, 0.15 mmol, 88 % yield). This crude product was used in preparing the metal complexes.

^{1}H NMR (400 MHz, THF) δ 7.44-7.23 (m, 5H, Ar-C*H*), 6.68 (s, 6H, Im-C*H*), 3.09 (s, 9H, Im-Me).

^{11}B NMR (400 MHz, THF) δ 0.6 (s, br).

Ce(C3)$_2$I

$CeI_3(thf)_{2.2}$ (100 mg, 0.15 mmol) and Li[C3] (100 mg, 0.15 mmol) were suspended in thf (5 mL) with stirring. After approximately 5 minutes all solid material had dissolved and a yellow-orange solution formed. Diethyl ether (6 mL) was added dropwise until a grey precipitate formed. The reaction mixture was filtered through a glass microfiber filter pipette. The solution was concentrated to 2 mL and a few drops of diethyl ether were added. This mixture was allowed to stand until orange crystals of **Ce(C3)$_2$I** formed; these were isolated from the solution by filtration and dried under vacuum (94 mg, 0.10 mmol, 69 % yield).

NMR:

^{1}H NMR (500 MHz, C_6D_6) δ 16.39 (4H, Ar-C*H*), 16.21 (6H, Im-C*H*), 10.93 (2H, Ar-C*H*), 10.22 (4H, Ar-C*H*), 6.91 (6H, Im-C*H*), 3.59 (2H, thf C*H$_2$*), 1.43 (2H, thf C*H$_2$*), -13.66 (18H, Im-Me).

^{11}B NMR (160 MHz, C_6D_6) δ 44.35 (s, br).

Elemental analysis (CHN):

Expected: C 46.52 %; H 4.34 %; N 18.08 %,

Found: C 46.76 %; H 4.61 %; N 17.83 %.

UV-Vis:

λ_{max}: 452nm, ε = 440 molL^{-1}cm^{-1}

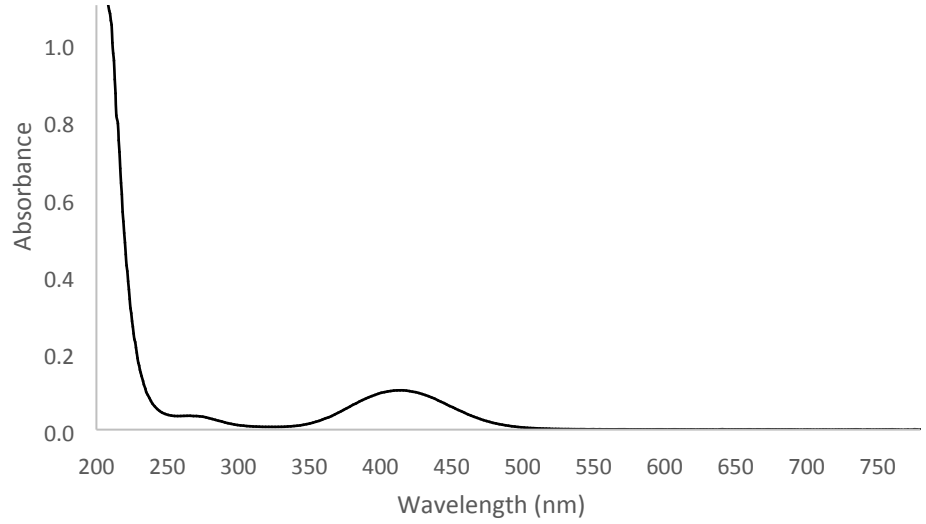

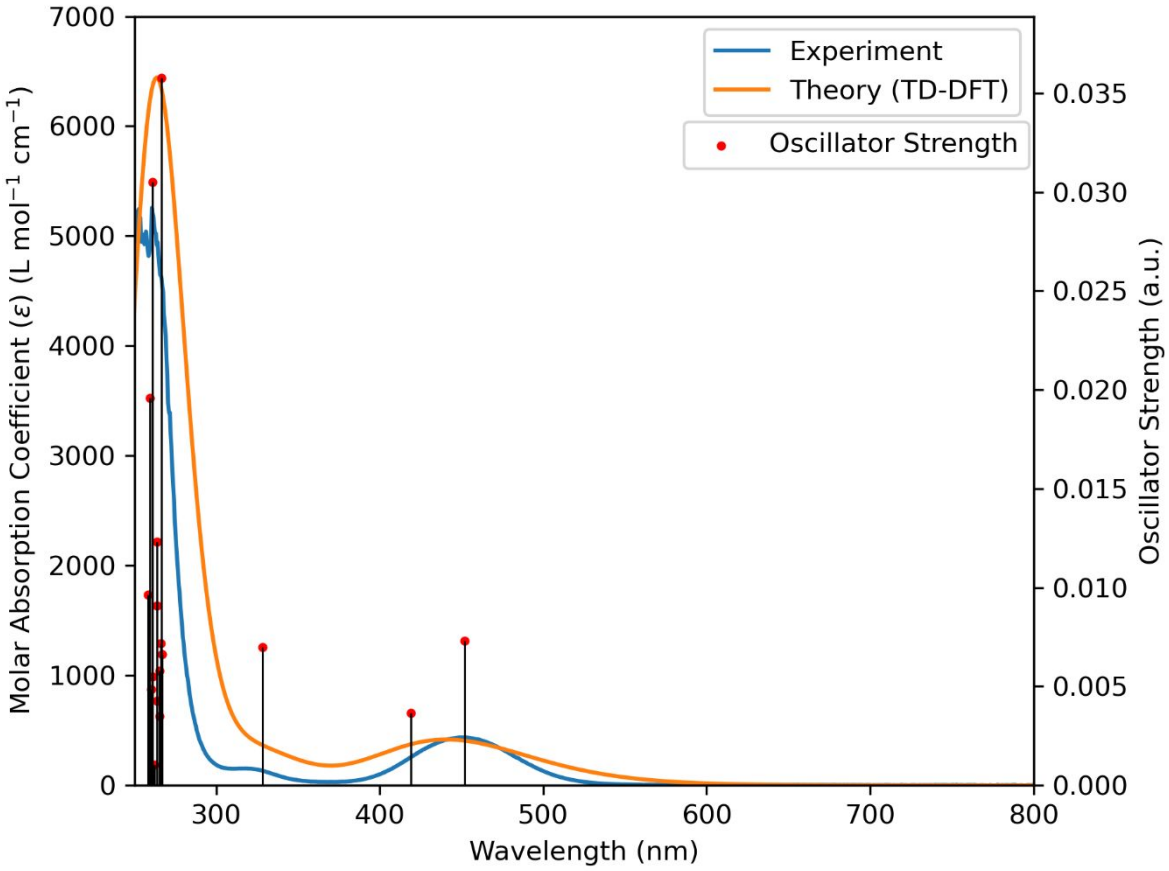

Figure S1: Comparison of calculated (orange) and experimental(blue) UV-Vis absorption spectra for **$Ce(C3)_2I$**

Thermal stability study of $Ce(C3)_2I$ complex:

$Ce(C3)_2I$ (10mg, 0.011 mmol) was dissolved in thf-d_8 (0.4 mL) in a Young's tap sealed NMR tube to give an orange-yellow solution. The resulting solution was heated to 66°C for 8 hours after which time a 1H-NMR spectrum was collected; no degradation was evident in the spectrum at this point (Spectrum 1, Figure 2). The sample was heated for a further 72 hours. Very minor degradation was observed to have occurred after this time (Spectrum 2, Figure 2).

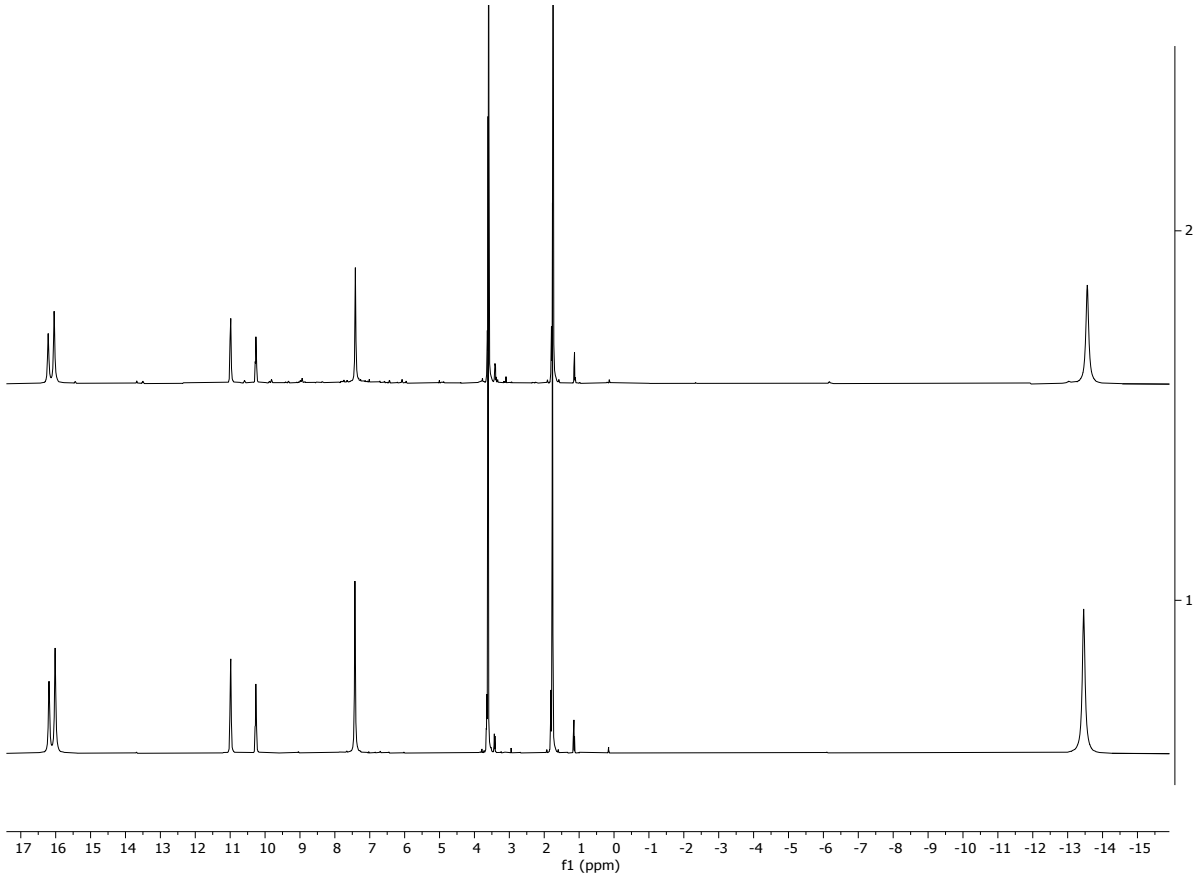

Figure S2: 1H-NMR spectra (400 MHz, 300K) of a sample of $Ce(C3)_2I$ in thf-d^8 after heating for 8 hours at 66°C (spectrum 1) and after 80 hours at 66°C (spectrum 2).

$[Li(thf)_4][CeC3I_3]$

$CeI_3(thf)_{2.2}$ (100 mg, 0.15 mmol) and **Li[C3]** (50 mg, 0.15 mmol) were suspended in thf (5 mL) with stirring. After two hours the resulting yellow solution was concentrated to approx. 1 mL in volume and toluene (1mL) was added. The solution was filtered and stored at -35°C overnight, resulting in crystallization of yellow needles suitable for single crystal X-ray diffraction. This solid was isolated via filtration and dried under vacuum, yielding **$[Li(thf)_4][CeC3I_3]$** (111 mg, 0.10 mMol, 66% yield).

NMR:

^{1}H NMR (500 MHz, C_6D_6) δ 15.49 (2H, Ar-C*H*), 13.96 (3H, Im-C*H*), 10.56 (2H, Ar-C*H*), 9.85 (1H, Ar-C*H*), 5.92 (16H, thf CH_2), 5.75 (Im-C*H*), 2.57 (16H, thf CH_2), -11.36 (9H, Im-Me).

^{11}B NMR (160 MHz, C_6D_6) δ -37.8 (s, br).

Elemental analysis (CHN):

Expected (**$[Li(thf)_4][CeC3I_3]. 0.5(C_7H_8)$**): C 38.60 %; H 4.82 %; N 6.93 %,

Found: C 38.30 %; H 4.74 %; N 6.44 %. Low in N, potentially due to boron nitride formation.

UV-Vis:

λ_{max}: 400 nm, ε = 1050 molL^{-1}cm^{-1}

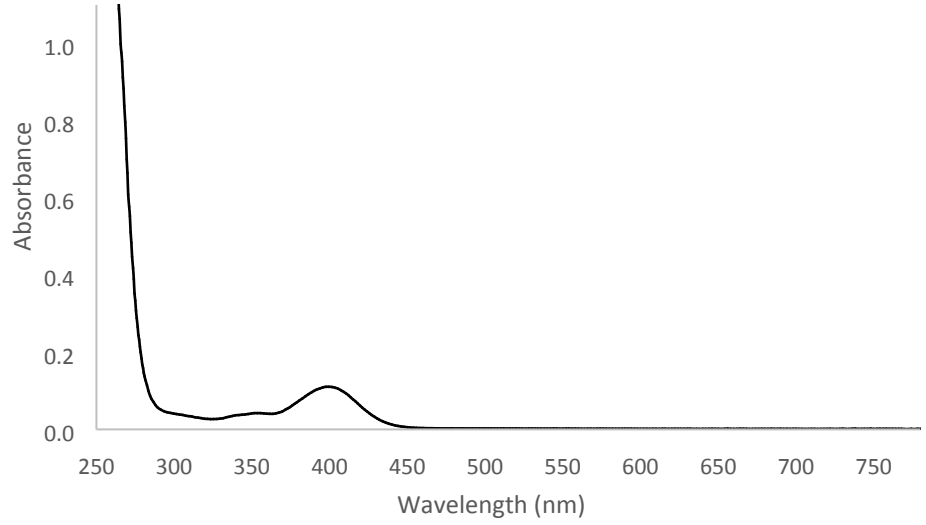

Ce(C3)$_2$bipy

Ce(C3)$_2$I (100mg, 0.11 mMol) was dissolved in thf (5 mL), to which K[bipy] (21 mg, 0.13 mMol) was added: the solution was observed to change color from orange to a deep red. The mixture was stirred for 2 hours, and then allowed to stand for 72 hours, during which time a white precipitate formed. The mixture was filtered, then concentrated to approximately 1 mL in volume, followed by addition of toluene (3 mL). After standing overnight, the reaction was again filtered and concentrated *in vacuo* to incipient crystallization. Upon standing at room temperature overnight a crop of an extremely air and moisture sensitive deep red microcrystalline solid was observed to have formed (48mg, 0.05 mMol, 46% yield). Crystals suitable for X-ray diffraction were grown from thf/toluene solutions of **Ce(C3)$_2$bipy**.

NMR:

^{1}H-NMR (400MHz, thf-d^{8}): 15.11 (9H Im-Me), 13.53 (3H Im-C*H*), 11.83 (9H, Im-Me), 10.76 (3H Im-C*H*), 8.21 (3H Im-C*H*), 8.19 (3H Im-C*H*), 8.10 (2H, bipy-C*H*), 8.01 (2H, bipy-C*H*), 7.70 (10H, overlapping Ar-C*H*), 5.19 (2H, bipy-C*H*), -0.19 (2H, bipy-C*H*).

^{11}B-NMR (128MHz, thf-d^{8}): δ 1.7 (s, br).

Elemental Analysis (**CHN**, **Ce(C3)$_2$bipy.thf**):

Expected: C, 58.26%; H, 5.48%; N, 19.02%.

Found: C, 58.01%; H, 5.08%; N, 18.64%.

UV-Vis:

Absorptions were observed at 937, 835, 758, 506 and 387nm with respective ε values of: 1910, 1860, 1170, 3490 and 15700 mol^{-1}Lcm^{-1}.

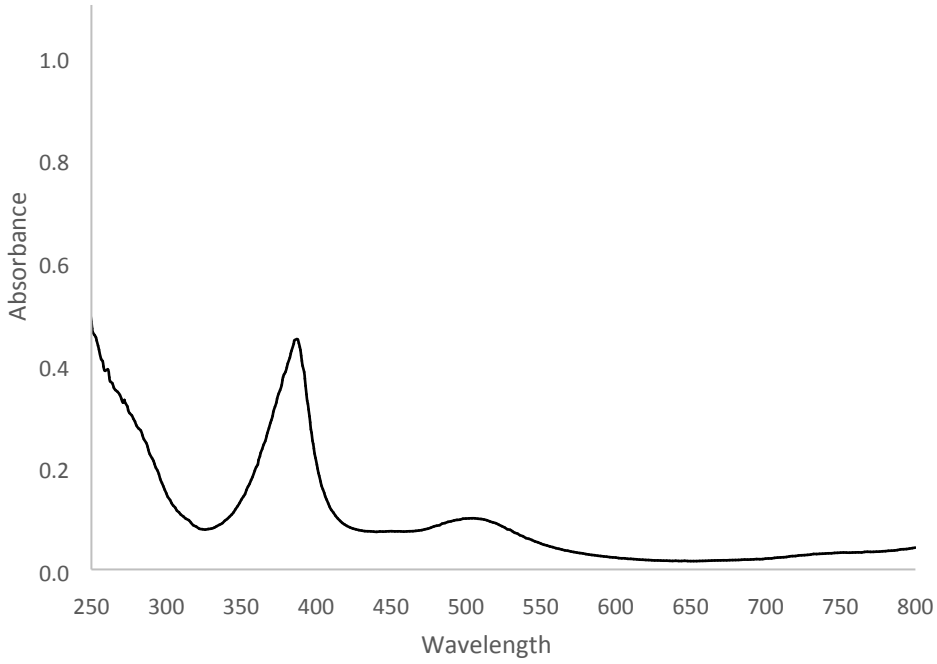
1.0
0.8
0.6
0.4
0.2
0.0
Absorbance
250 300 350 400 450 500 550 600 650 700 750 800
Wavelength

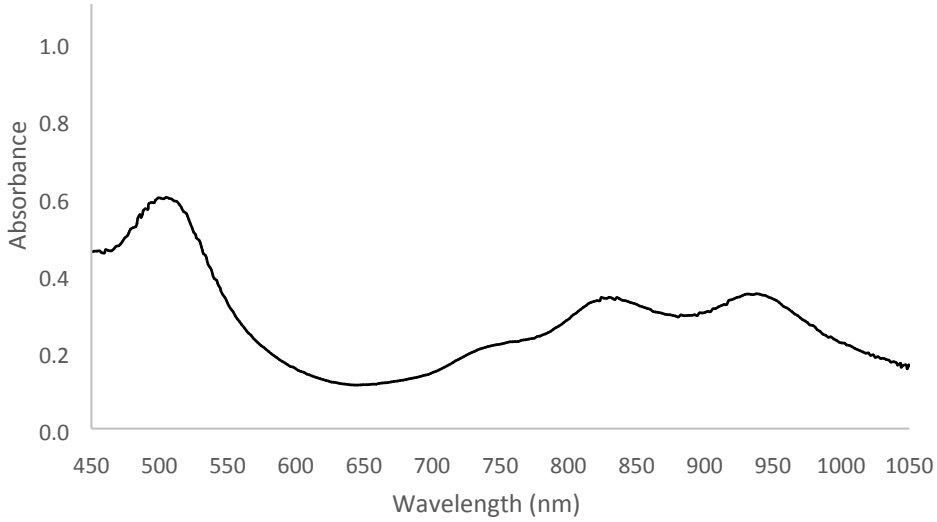
1.0
0.8
0.6
0.4
0.2
0.0
Absorbance
450 500 550 600 650 700 750 800 850 900 950 1000 1050
Wavelength (nm)

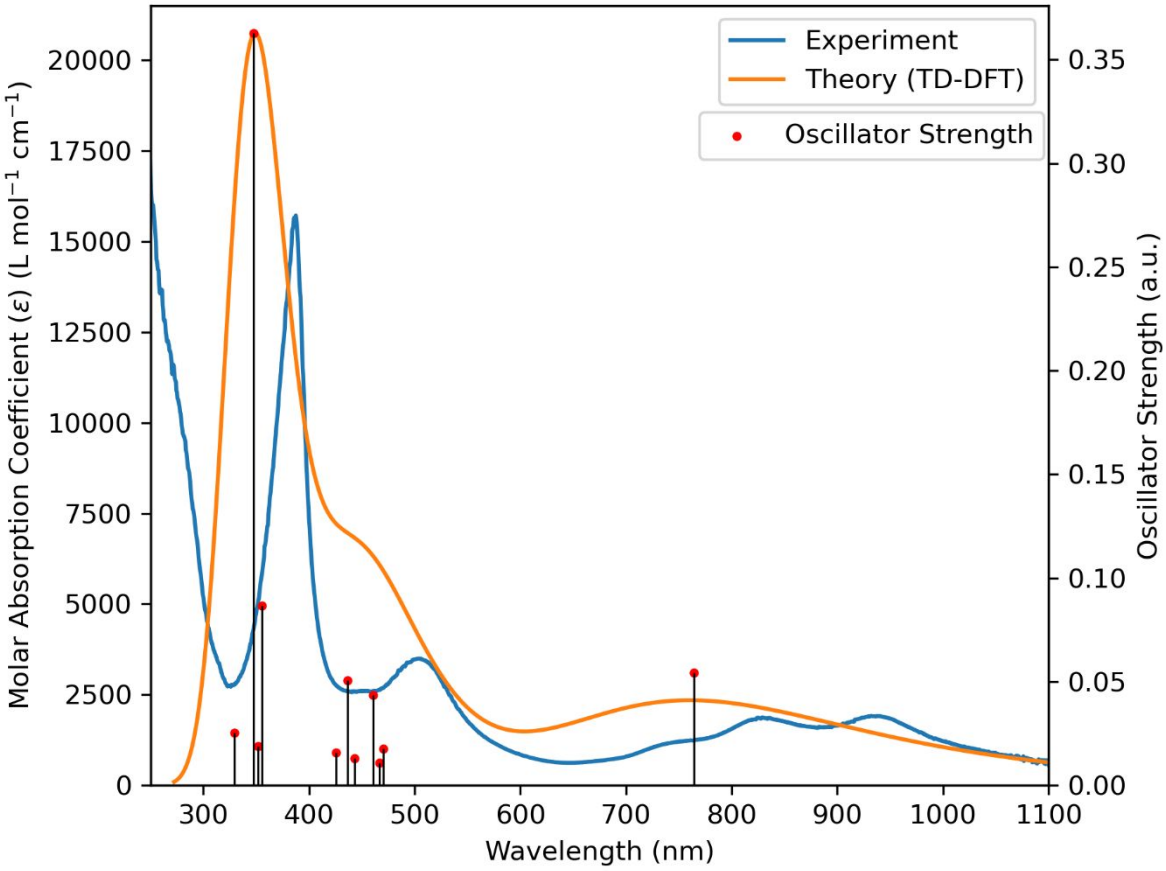

Figure S3: Comparison of calculated (orange) and experimental(blue) UV-Vis absorption spectra for **Ce(C3)$_2$bipy**

Testing the lability of the Ce – bound [C3]$^-$ ligand:

The addition of two equivalents of **Li[C3]** (5.2 mg, 0.16 mmol) to $CeI_3thf_{2.2}$ (5 mg, 0.0078 mmol) in thf (0.4 mL) led to the formation of a pale-orange/yellow solution almost immediately. A range of ^{1}H-NMR resonances are observed for this solution between 16.2—13.6 ppm by no-D ^{1}H-NMR corresponding to **Ce(C3)$_2$I**. The addition of a further equivalent of $CeI_3thf_{2.2}$ (5 mg, 0.0078 mmol) rapidly results in the formation of the pale yellow solution associated with **[Li(thf)$_4$][Ce(C3)I$_3$]**; corresponding resonances between 14.8 and -10.4 ppm in the ^{1}H-NMR spectrum were observed. This can be reversed through the addition of a further equivalent of **Li[C3]** (5.2 mg, 0.16 mmol) again over a period of minutes, giving **Ce(C3)$_2$I** (1H-NMR signals again observed between 16.2-13.6 ppm).

Yb(C3)$_2$I

Li[C3] (0.24 g, 0.71 mmol) was added to $YbI_3(thf)_{2.5}$ (0.25 g, 0.35 mmol) in thf (7 mL); the resulting suspension was stirred at room temperature for 30 minutes, then left to stand for one hour, after which time dme (5 mL) was added, giving an off-white solid. The reaction was filtered, retaining the solid. The solid was extracted into dcm (4 mL) to remove salts and swiftly filtered (slow degradation of the desired

product occurs in dcm), followed by removal of the solvent *in vacuo*. The resulting solid (0.11 g, 0.11 mmol, 33% yield) was determined to be $[Yb(C3)_2]I$. Colorless single crystals suitable for X-ray diffraction could be grown directly from small scale reactions of Li[C3] (9 mg, 0.026 mmol) and $YbI_3(thf)_{2.5}$ (10 mg, 0.014 mmol) in thf (0.4 mL) that were allowed to stand overnight.

NMR:

^{1}H NMR (400 MHz, CD_2Cl_2) δ 31.15 (18H, Im-Me), 9.39 (6H, Im-C*H*), 2.30 (2H, Ar-C*H*), 1.03 (4H, Ar-C*H*), -5.64 (Im-C*H*), -7.57(4H, Ar-C*H*).

^{11}B NMR (128 MHz, CD_2Cl_2) δ -74.88 (s, br).

Elemental Analysis (**CHN**):

Expected: C, 44.93%; H, 4.19%; N, 17.47%.

Found: C, 44.72%; H, 4.14%; N, 17.21%.

SAMBVCA 2.1 steric profile analysis of Tp* vs C3 in $[YbL_2]X$ complexes

The SAMBVCA applet 2.1 was used to estimate the volume that one **[C3]**$^-$ or Tp* ligand occupies around around a Yb(III) ion within a sphere of 3.5 Å radius, centered on the metal centre (%V_Bur).[9] Coordinates for the ligands were taken from complexes of the structure $[YbL_2]X$ where X is an outersphere anion (I^-, $^-$OTf) and L = Tp* or C3). The coordinates used for the Tp* ligand for Yb were taken from CCDC structure 1234400[10] and are given below while the coordinates for the **[C3]**$^-$ ligand were taken from the structure reported here for **$Yb[C3]_2I$**. All default parameters in the SAMBVCA applet were used as found, unless otherwise stated.

Method:

1) The coordinate file was loaded into the applet.

2) Yb was set as the centre of the sphere

3) The z-axis was defined by clicking on Yb (0) and B(10) for the Tp* ligand, and Yb(0) and B(24) for the C3 ligand.

4) The xz-plane was defined by clicking on Yb(0), N(1), N(4) and B(10) for the Tp* ligand, and Yb(0), C(16), N(4) and B(24) for the C3 ligand.

5) The Yb(0) atom was deleted.

5) The Bondi van der Waals radii were scaled by 1.17 (applet default).

6) The sphere radius was set to 3.5 Å (applet default).

7) The distance of the coordination point from the centre of the sphere was set to 0.

8) The mesh spacing for numerical integration was set to 0.10 (applet default) and the job was then submitted to the applet

Coordinates for Tp* ligand coordinated to a Yb center:

Yb	0.00000	0.00000	0.00000
N	-1.12302	-1.47920	1.36293
N	-1.12302	1.47920	1.36293
N	-2.02999	-0.00000	-1.17934
N	-2.45884	-1.26183	1.59460
C	-0.85579	-2.70412	1.87523
N	-2.45884	1.26183	1.59460
C	-0.85579	2.70412	1.87523
N	-3.18095	-0.00000	-0.45548
C	-2.40137	-0.00000	-2.44960
B	-3.16448	0.00000	1.09454
C	-2.96951	-2.31587	2.21094
C	-1.97754	-3.22772	2.39278
C	0.53073	-3.24139	1.78344
C	-2.96951	2.31587	2.21094
C	-1.97754	3.22772	2.39278
C	0.53073	3.24139	1.78344
C	-4.22540	-0.00000	-1.28862
C	-3.76094	-0.00000	-2.54314
C	-1.39184	-0.00000	-3.56075
C	-4.40848	-2.41840	2.56675
C	-4.40848	2.41840	2.56675
C	-5.63128	-0.00000	-0.81478

Coordinates for C3 ligand on Yb center:

Yb	7.06785	9.57488	24.83233
N	4.20741	8.39311	23.15215
N	5.05289	12.19330	24.94739
N	8.35993	11.55311	22.18477

N	4.36213	10.54054	23.13130
N	6.31861	12.05851	22.69632
N	5.63085	11.96712	27.01124
C	3.38689	8.81831	22.13786
C	3.88599	13.14976	22.87994
C	3.49470	10.16708	22.11421
C	2.50349	12.95426	23.00862
C	4.30025	13.08905	25.70590
C	4.30224	14.43585	22.49387
C	6.63703	12.70572	21.51646
C	9.67655	10.93220	22.17074
C	5.87940	11.48210	25.76564
C	4.83428	9.43067	23.76192
C	7.38668	11.30369	23.11767
C	4.38509	6.98144	23.51617
C	7.91173	12.40130	21.20777
C	4.65860	12.94834	26.99520
C	1.58315	13.95697	22.71597
C	3.38190	15.43154	22.17475
C	2.03034	15.19528	22.28139
B	4.90316	12.00153	23.39269
C	6.32060	11.51958	28.21435

Results of the SAMBVCA 2.1 analysis:

For $Yb^{III}(Tp^*)$:

%V Free	%V Buried	% V Tot/V Ex
52.1	47.9	99.9

Quadrant	V f	V b	V t	%V f	%V b
SW	21.1	23.8	44.9	47.0	53.0
NW	20.6	24.2	44.9	46.0	54.0
NE	25.7	19.1	44.9	57.4	42.6
SE	26.1	18.8	44.9	58.1	41.9

Steric Map

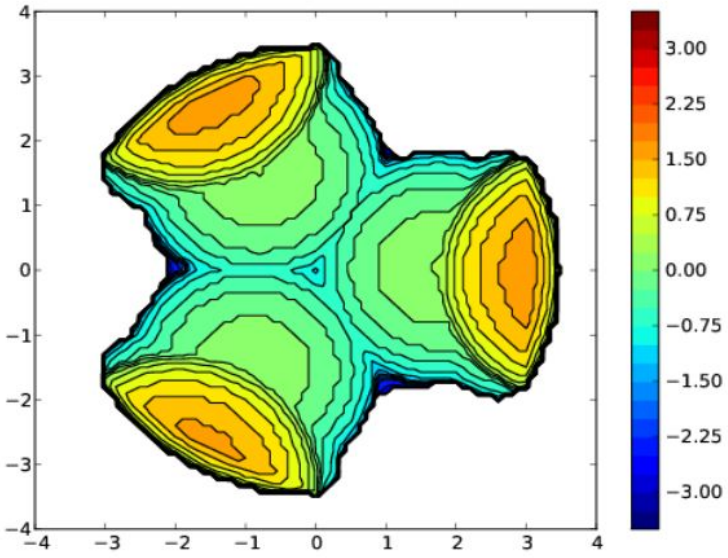

For Yb[C3]$_2$I:

%V Free	%V Buried	% V Tot/V Ex
53.5	46.5	99.9

Quadrant	V f	V b	V t	%V f	%V b
SW	21.9	22.9	44.9	48.9	51.1
NW	21.5	23.4	44.9	47.9	52.1
NE	26.9	18.0	44.9	59.9	40.1
SE	25.8	19.1	44.9	57.4	42.6

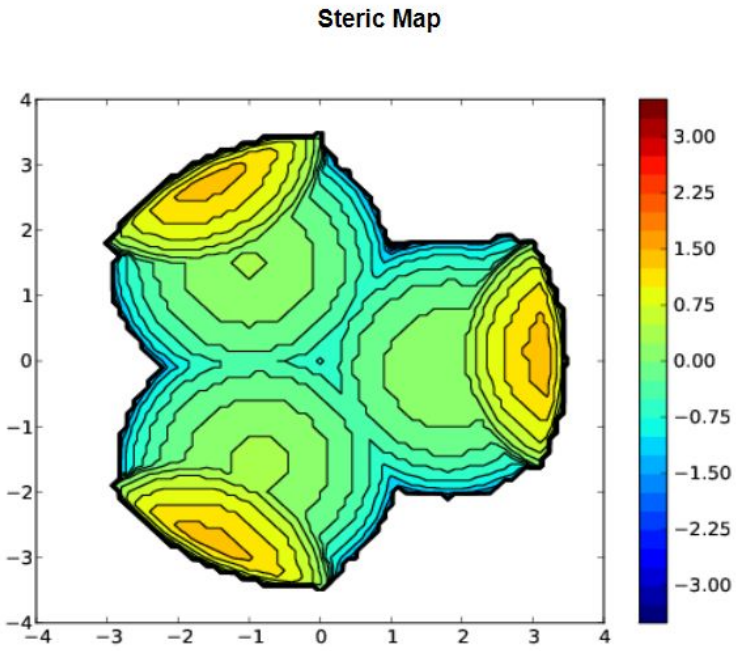

The percent buried volume (%VBur) of the Tp* ligand around the Yb(III) center is calculated to be 47.9 %VBur, while that for C3 around a Yb(III) center is 46.5 %VBur, showing the similar steric bulk of the two ligand sets. The maps showing the distribution of steric bulk around the metal center are also similar for Tp* and C3, with the distribution of steric bulk being similar in each of the 4 quadrants around the metal center within a sphere of 3.5 Å radius.

Crystallography

Cifs are deposited with the CCDC with codes 2235950-2235953.

Additional information for the structure of $[Li(thf)_4][Ce(C3)I_3]$.

$[Li(thf)_4][Ce(C3)I_3]$ crystallizes as an ion pair in the $P2_1/c$ space group with Z=4 (Figure 2). The Ce-C distances range between 2.591(3) to 2.662(3) Å, which are comparable to the distances observed for the Ce-C bonds in **$Ce(C3)_2I$** (range 2.631(2)-2.781(2) Å). The Ce-I distances range from 3.1324(3) to 3.1428(3) Å for **$[Li(thf)_4][Ce(C3)I_3]$**, which are slightly shorter than that seen in **$Ce(C3)_2I$** (3.2951(2) Å), presumably due to reduced steric hindrance about Ce.

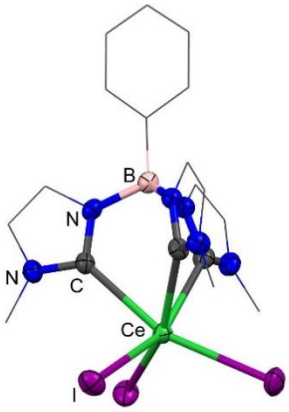

Figure S4: Solid-state structure of $[Li(thf)_4][Ce(C3)I_3]$; thf-coordinated lithium counterion and disordered co-crystallized toluene omitted for clarity. Phenyl and backbone carbons set respectively to wireframe and capped sticks; hydrogens are omitted for clarity. C= grey, Ce= green, N=blue B=pink, I=purple.

Crystallographic data tables

Compound	**$Ce(C3)_2I$**
Empirical formula	$C_{36}H_{40}B_2N_{12}ICe$
Formula weight	929.44
Temperature/K	100.00(11)
Crystal system	monoclinic
Space group	$P2_1/n$
a/Å	8.61860(10)
b/Å	21.6975(3)
c/Å	20.3758(3)
α/°	90
β/°	92.7150(10)
γ/°	90
Volume/Å³	3806.04(9)
Z	4
$\rho_{calc}g/cm^3$	1.622
μ/mm^{-1}	2.051
F(000)	1844.0
Crystal size/mm³	0.3 × 0.16 × 0.06
Radiation	Mo Kα (λ = 0.71073)
2Θ range for data collection/°	4.002 to 52.74

Index ranges	-10 ≤ h ≤ 10, -27 ≤ k ≤ 27, -25 ≤ l ≤ 25
Reflections collected	79661
Independent reflections	7779 [R_{int} = 0.0425, R_{sigma} = 0.0191]
Data/restraints/parameters	7779/0/475
Goodness-of-fit on F^2	1.051
Final R indexes [I>=2σ (I)]	R_1 = 0.0217, wR_2 = 0.0481
Final R indexes [all data]	R_1 = 0.0265, wR_2 = 0.0498
Largest diff. peak/hole / e $Å^{-3}$	0.87/-0.53

Compound	**$[Yb(C3)_2]I$**
Empirical formula	$C_{36}H_{40}B_2IN_{12}Yb$
Formula weight	962.36
Temperature/K	100.00(13)
Crystal system	orthorhombic
Space group	Pbcm
a/Å	9.98200(10)
b/Å	21.9170(2)
c/Å	40.0903(3)
α/°	90
β/°	90
γ/°	90
Volume/$Å^3$	8770.78(14)
Z	8
ρ_{calc}g/cm^3	1.458
μ/mm^{-1}	9.771
F(000)	3784.0
Crystal size/mm^3	0.16 × 0.115 × 0.052
Radiation	Cu Kα (λ = 1.54184)
2Θ range for data collection/°	8.068 to 148.996
Index ranges	-12 ≤ h ≤ 12, -27 ≤ k ≤ 17, -50 ≤ l ≤ 48
Reflections collected	160321
Independent reflections	9095 [R_{int} = 0.0580, R_{sigma} = 0.0211]
Data/restraints/parameters	9095/0/477
Goodness-of-fit on F^2	1.044
Final R indexes [I>=2σ (I)]	R_1 = 0.0408, wR_2 = 0.0951
Final R indexes [all data]	R_1 = 0.0425, wR_2 = 0.0962
Largest diff. peak/hole / e $Å^{-3}$	1.29/-0.91

Compound	**$[Li(thf)_4][Ce(C3)I_3]$**
Empirical formula	$C_{41}H_{60}BCeI_3LiN_6O_4$
Formula weight	1239.52
Temperature/K	100.00(10)
Crystal system	monoclinic
Space group	$P2_1/c$
a/Å	11.0280(2)

b/Å	13.4919(2)
c/Å	33.1783(6)
α/°	90
β/°	98.164(2)
γ/°	90
Volume/Å³	4886.53(15)
Z	4
ρ_{calc}*g/cm³*	1.685
μ/mm⁻¹	2.870
F(000)	2420.0
Crystal size/mm³	0.32 × 0.225 × 0.077
Radiation	Mo Kα (λ = 0.71073)
2Θ range for data collection/°	3.264 to 52.738
Index ranges	-13 ≤ h ≤ 13, -16 ≤ k ≤ 16, -41 ≤ l ≤ 41
Reflections collected	102572
Independent reflections	10000 [R_{int} = 0.0482, R_{sigma} = 0.0222]
Data/restraints/parameters	10000/1204/767
Goodness-of-fit on F²	1.030
Final R indexes [I>=2σ (I)]	R_1 = 0.0295, wR_2 = 0.0676
Final R indexes [all data]	R_1 = 0.0378, wR_2 = 0.0720
Largest diff. peak/hole / e Å⁻³	1.98/-1.44

Complex	**$Ce(C3)_2bipy$**
Empirical formula	$C_{53}H_{56}B_2CeN_{14}$
Formula weight	1050.85
Temperature/K	100.00(10)
Crystal system	monoclinic
Space group	$P2_1/c$
a/Å	27.31031(17)
b/Å	8.65621(4)
c/Å	22.48352(12)
α/°	90
β/°	109.4313(7)
γ/°	90
Volume/Å³	5012.44(5)
Z	4
ρ_{calc}*g/cm³*	1.393
μ/mm⁻¹	7.422
F(000)	2160.0
Crystal size/mm³	0.422 × 0.085 × 0.064
Radiation	Cu Kα (λ = 1.54184)
2Θ range for data collection/°	6.864 to 149.008
Index ranges	-33 ≤ h ≤ 33, -10 ≤ k ≤ 10, -28 ≤ l ≤ 28
Reflections collected	187985

Independent reflections	10234 [R_{int} = 0.0665, R_{sigma} = 0.0202]
Data/restraints/parameters	10234/385/703
Goodness-of-fit on F^2	1.053
Final R indexes [I>=2σ (I)]	R_1 = 0.0236, wR_2 = 0.0633
Final R indexes [all data]	R_1 = 0.0245, wR_2 = 0.0639
Largest diff. peak/hole / e $Å^{-3}$	0.77/-0.78

Computational Methods and Additional Information

All quantum chemistry computations were performed using the unrestricted B3LYP[11-13] hybrid density functional augmented with Grimme's D4[14, 15] dispersion scheme using the Orca 5.0.3[16] program package. The tetrahydrofuran (THF) solvent environment was modeled using the SMD[17] implicit solvent scheme. The metal complex geometries were optimized using the double zeta Karlsruhe basis set, def2-SVP[18, 19] on the ligand atoms and the corresponding triple zeta basis (def2-TZVP[18, 19]) on the metal center, which automatically assigns def2-ECP[20] pseudopotential for the core electrons of the heavier elements (viz., Yb, Ce, and I in the present work). To obtain accurate electronic energies (and hence, binding energies), single-point energy calculations were performed on the optimized structures with the triple zeta basis set, def2-TZVP, on all the atoms. The metal-ligand bonding character was analyzed using various QTAIM[21] metrics, which were computed using the Multiwfn[22] software. Furthermore, accurate partial atomic charges were computed using the natural population analysis (NPA) scheme implemented within the NBO 7.0[23] framework. The theoretical UV-Vis spectra for DFT-optimized Ce complexes were simulated using the time-dependent density functional theory (TD-DFT) method incorporating 50 excited states utilizing the B3LYP-D4/def2-TZVP level of theory and the implicit THF solvation scheme. The TD-DFT computed UV-Vis spectra were analyzed using the Multiwfn package.

Table S1. QTAIM and NPA charges for the metal atoms in the optimized lanthanide borate systems

Complex	Metal atom	QTAIM Charges	NPA Charges (From NBO)
$Ce(C3)_2I$	Ce	2.01	1.34
$Ce(C3)_2(bipy)$	Ce	2.04	1.32
$Ce(Tp^*)_2(bipy)$	Ce	2.19	1.73
$[Yb(C3)_2]I$	Yb	2.10	1.63
$[Yb(Tp^*)_2]I$	Yb	2.24	1.96

(HOMO-1) Alpha to (HOMO-4) Alpha Molecular Orbitals for Lanthanide Borate Complexes

1) $Ce(C3)_2I$

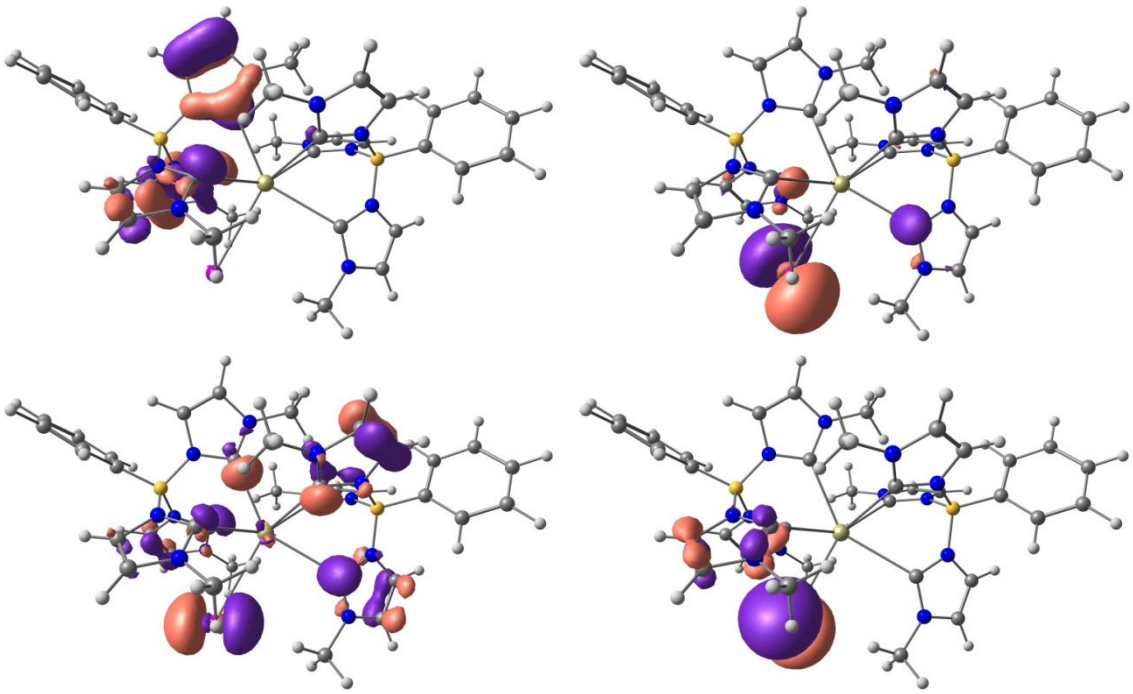

2) $Ce(C3)_2bipy$

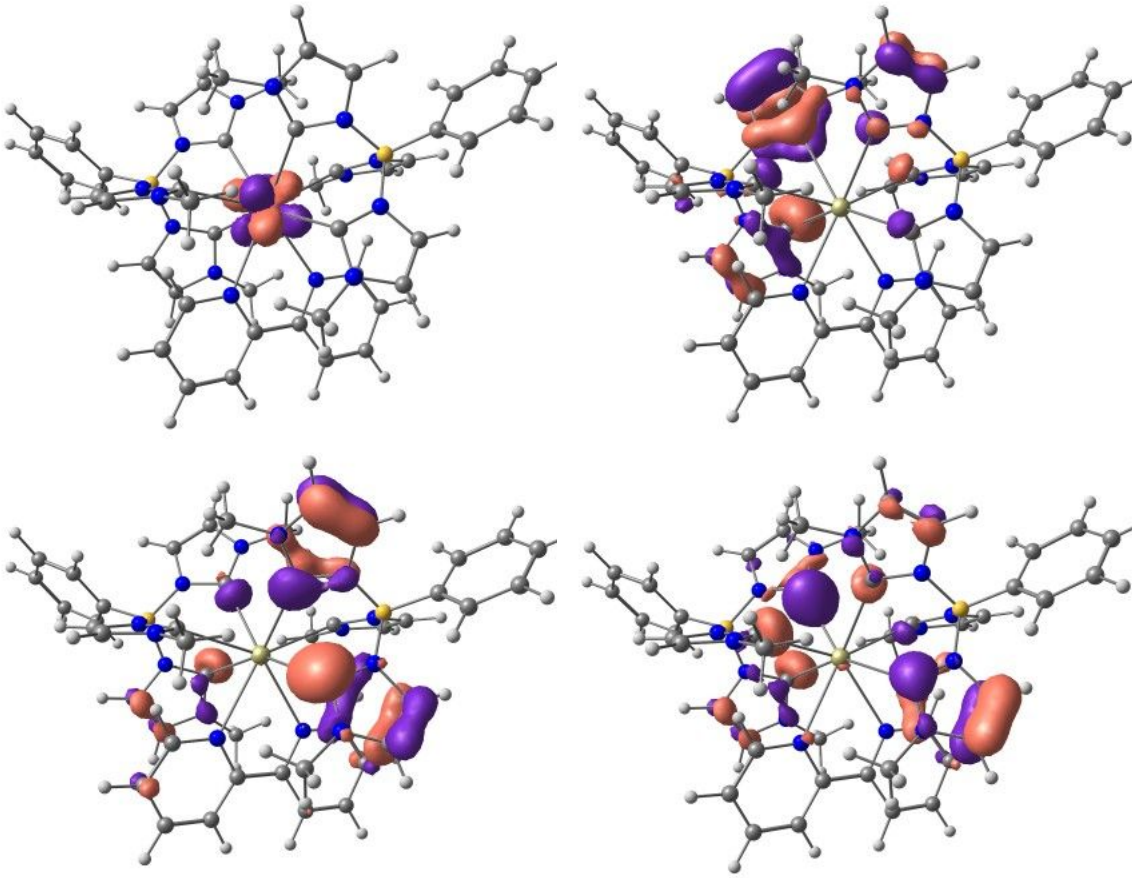

3) $Ce(Tp^*)_2bipy$

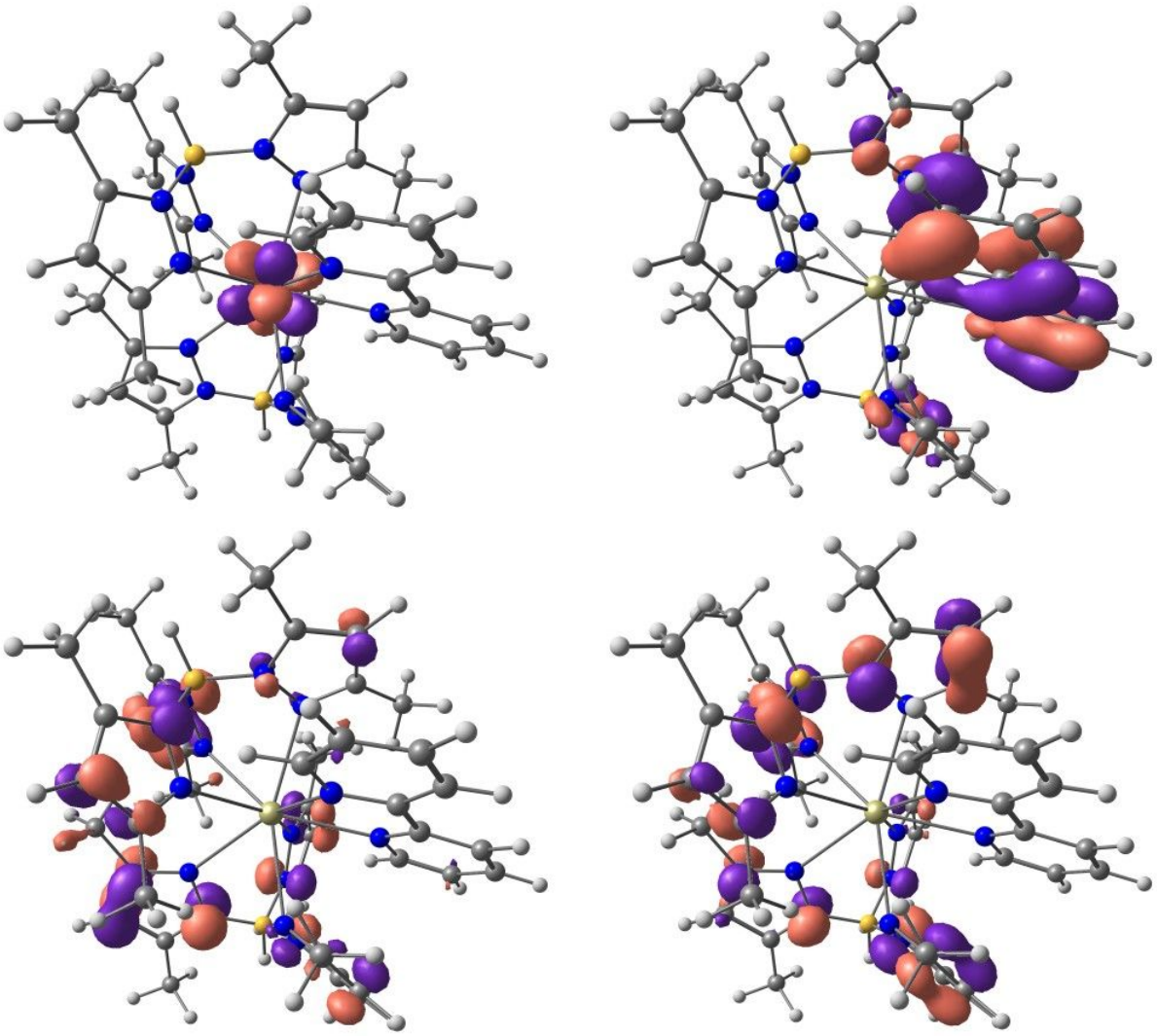

4) [Yb(C3)$_2$]I (MOs localized on the Iodine ion were ignored)

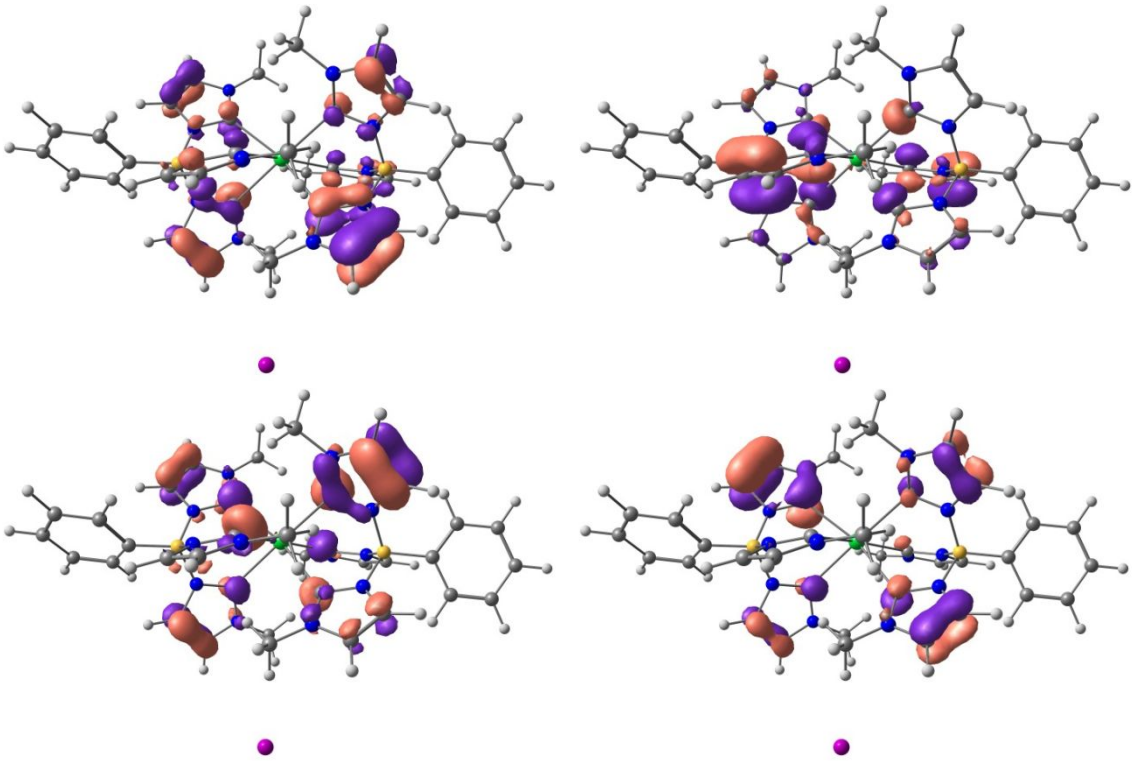

5) [Yb(Tp*)$_2$]I (MOs localized on the Iodine ion were ignored)

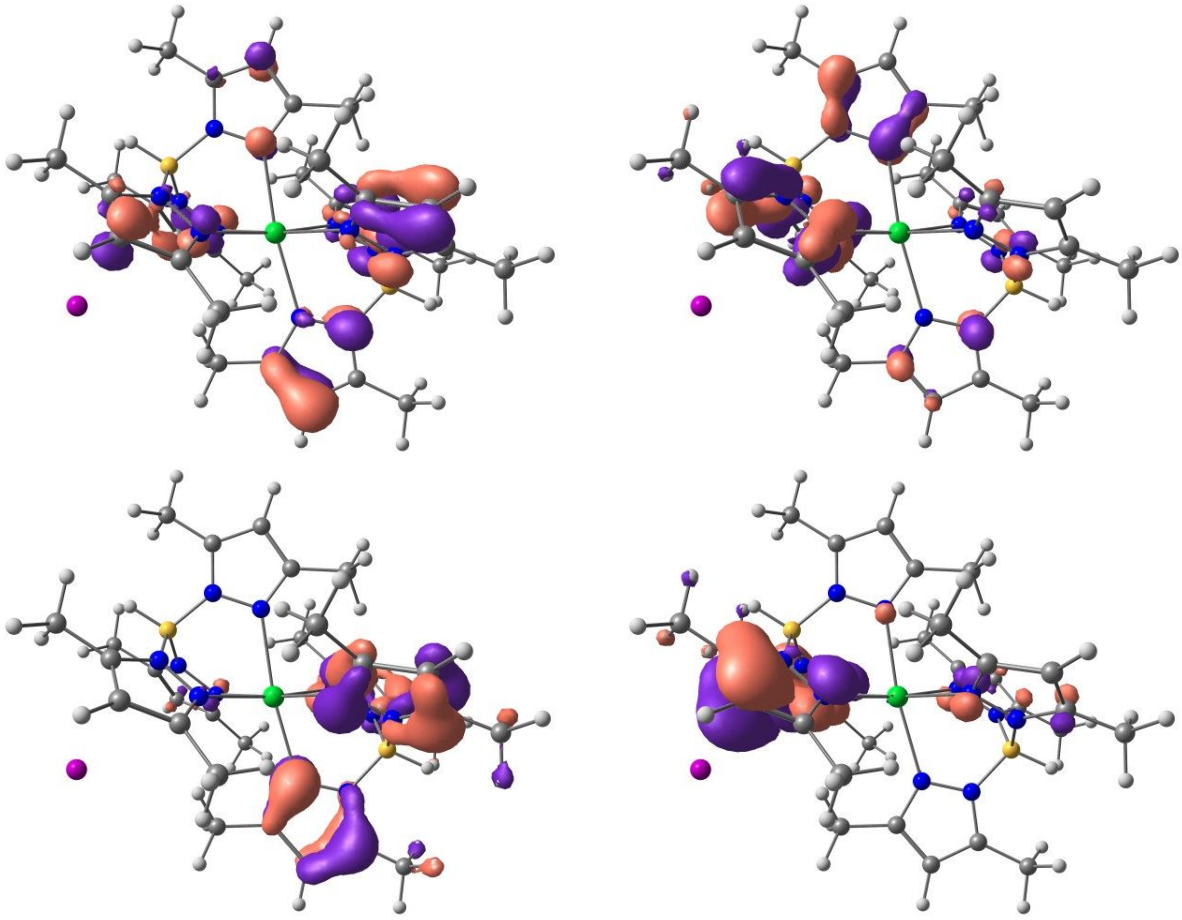

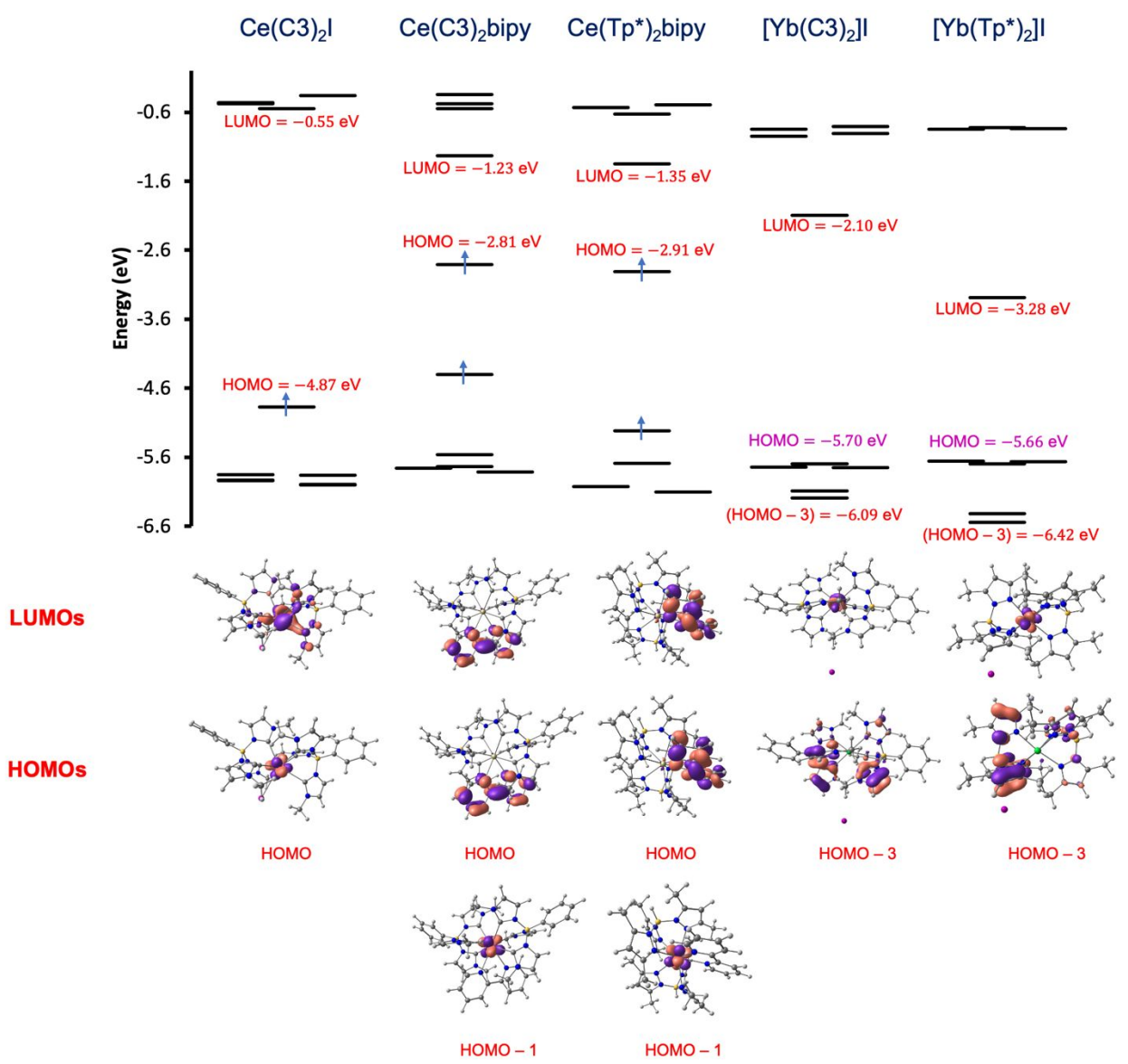

Figure S5. Calculated frontier molecular orbital diagrams for lanthanide borate complexes. The three nearly degenerate HOMOs for the Yb complexes (shown in magenta) are exclusively localized on the non-bonded iodine ion.

Additional discussion of electronic structure for Ce(C3)$_2$I, Ce(C3)$_2$bipy:

As shown in Figure 5, for **Ce(C3)$_2$bipy** both the HOMO and LUMO are delocalized over the bipyridyl ligand with a predominantly p-character. The (HOMO-1) orbital, on the other hand, is entirely 4f in character, representing the unpaired electron on the metal center. As expected, the SOMO of **Ce(C3)$_2$I** is the electron located in a cerium 4f-orbital. More interestingly, the LUMO is a hybrid of p (52%), d (34%), and f (10%) orbitals, with major contributions from the metal center and the carbene carbons. The Ce-I bond is primarily ionic, as there was no observed overlap between Ce and I in any occupied molecular orbitals.

UV-Vis Spectra Analysis

The UV-Vis absorption spectra of $Ce(C3)_2I$ and $Ce(C3)_2bipy$ were obtained using the time-dependent density functional theory (TD-DFT) method and were compared with the experimental spectra. As illustrated in Figures 1 and 3, the TD-DFT computed spectra reproduce all the major peaks in the experimental spectra, validating the theoretical predictions. In this study, we further analyze each of the UV-Vis peaks to understand their origins. By identifying the contributions of the individual excited states or transitions, we gain a deeper insight into the electronic structure of the two complexes and the nature of the electronic transitions that occur upon excitation. Figure 6 illustrates the TD-DFT computed UV-Vis spectra of the two complexes, along with the individual transition curves, which provide insight into the contribution of each transition to a particular peak in the spectrum. The absorption spectrum of $Ce(C3)_2I$ exhibited two major peaks at 263.4 nm and 440.6 nm, as depicted in Figure 6a. The highly intense peak at 263.4 nm was found to have contributions from multiple excited states, specifically transitions S35, S47, S49, and S42, with a contribution percentage ranging from 7% to 22%. The transitions were found to be delocalized across multiple molecular orbitals. The second peak at 440.6 nm was observed to be mostly composed of the S0→S7 transition (68.8%), which is mainly associated with the α-HOMO to α-LUMO transition. The remaining intensity (30.9%) was assigned to the S8 excited state, which mainly corresponds to the α-HOMO to α-(LUMO+1) transition (47.6%). A small shoulder peak at 328.3 nm in the absorption spectrum was observed and was found to be exclusively attributed to the S0→S9 transition. This transition involves multiple molecular orbital transitions, with the primary contributions coming from the α-HOMO to α-(LUMO+2) transition (12.2%) and the α-HOMO to α-(LUMO+10) transition (13.7%).

The UV-Vis absorption spectrum of $Ce(C3)_2bipy$ was analyzed to reveal two major peaks at 348.8 nm and 760.8 nm. As illustrated in Figure 6b, the peak at 348.8 nm was found to be mostly composed of the S0→ S37 transition (70.6%), with a minor contribution from the S0→S33 transition (16.4%). Further analysis revealed that the S37 excited state is primarily composed of a β-HOMO to β-LUMO transition (50%). The second peak at 760.8 nm was found to be almost exclusively associated with the S8 excited state (93.4%), which is predominantly characterized by a transition from α-HOMO to α-(LUMO+1) (83%). A broad peak was also observed at around 445 nm in the absorption spectrum, with almost equal contributions from the S20 and S22 excited states, primarily composed of the α-HOMO to α-(LUMO+12) (59%) and α-HOMO to α-(LUMO+15) (45%) transitions, respectively.

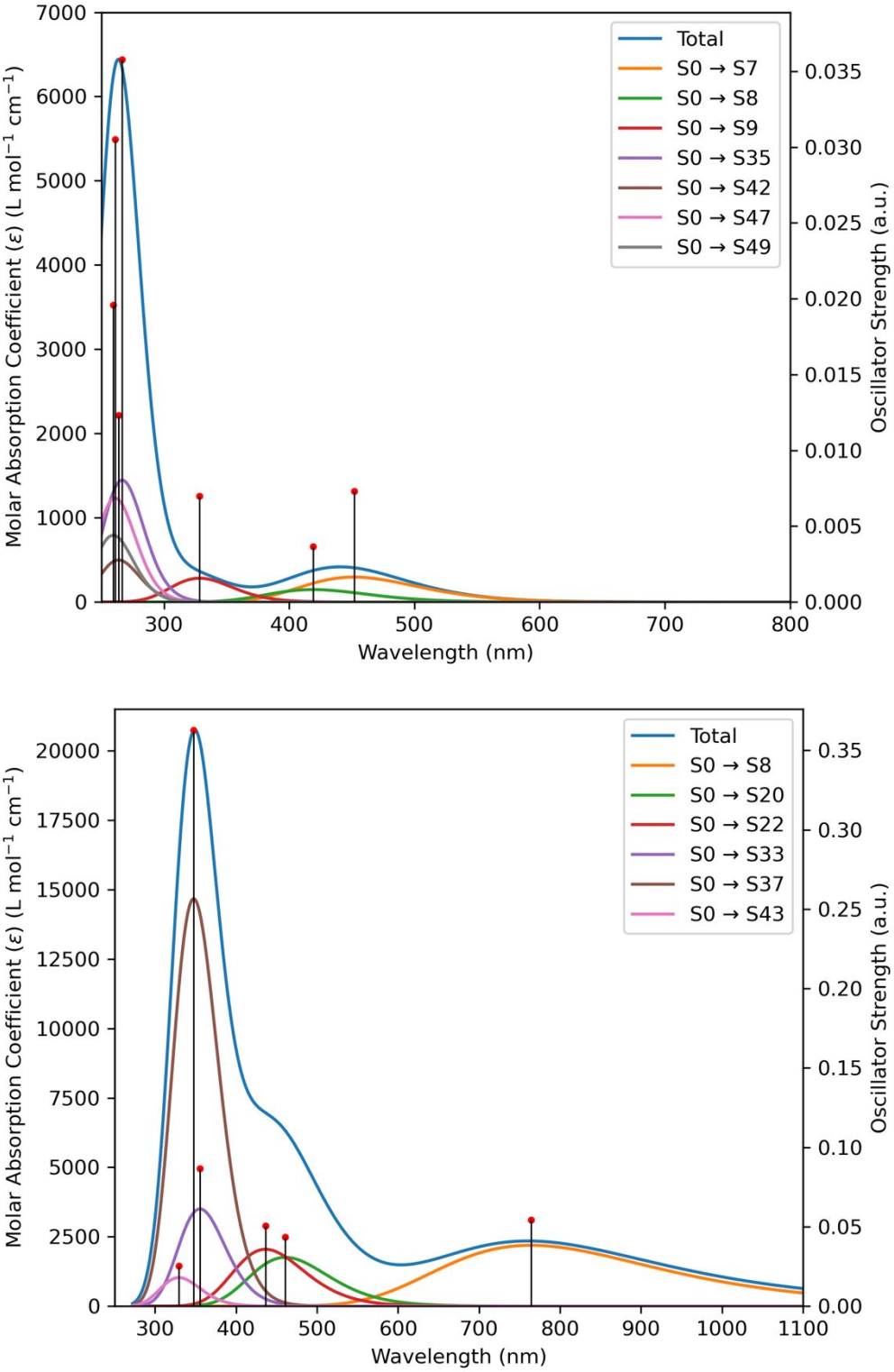

Figure 6. TD-DFT computed UV-Vis spectrum of **(a)** $Ce(C3)_2I$ **(b)** $Ce(C3)_2bipy$ with individual transition (or excited state) contributions.

Optimized Cartesian Coordinates for the Lanthanide Borate Complexes

1) $Ce(C3)_2I$

Ce	-0.157819	6.377283	11.522108
C	0.800199	3.862642	11.625017
N	1.086684	8.468456	14.102477
N	1.070711	9.756535	11.862178
C	1.071261	7.163520	13.708698
C	0.102238	11.398382	15.311082
C	2.060432	11.721581	13.973597
C	0.858616	11.018979	14.184032
C	0.492266	12.445910	16.151389
C	1.674820	13.146608	15.896028
B	0.484689	9.695052	13.315992
C	2.464465	12.771167	14.805842
C	1.411761	8.695755	11.073240
N	-1.718602	3.694649	13.231851
N	-1.689072	5.239334	14.748401
N	-2.961536	8.668823	12.500439
N	-1.069062	9.518858	13.113756
N	1.953489	3.437704	11.041913
N	-2.350656	3.680859	10.735914
N	-0.086986	2.846789	11.443710
N	1.691024	6.475264	14.702267
C	-1.547141	6.502051	15.452687
C	-1.630831	8.392349	12.590217
C	-2.225002	1.427686	12.123967
B	-1.596725	2.905182	11.878372
C	0.495418	1.837946	10.695548
N	1.796382	9.261194	9.890679
C	1.879849	5.036038	14.739411
C	-3.233792	9.957696	12.919703
C	1.645299	10.634622	9.911554
C	2.096800	7.322848	15.716669
C	-2.197773	3.133037	14.408036
C	1.716342	8.572944	15.337566
C	-3.613982	1.206381	12.040881
C	-3.208278	6.563556	8.808779
C	-2.321126	5.032304	10.565965
C	-2.991928	3.082614	9.663171
C	1.787390	2.200968	10.449784
C	1.171686	10.940786	11.150697
C	-3.419991	4.075743	8.833168
C	-3.992847	7.726832	12.102051
C	-2.181772	4.101018	15.362961
C	-2.037069	10.493166	13.291261
C	-2.010520	-0.878444	12.941068
C	2.373608	8.557832	8.758883
I	0.451971	5.375455	8.294702
C	-4.192131	-0.021759	12.376656
C	3.170704	4.223066	10.962207
N	-3.007918	5.260010	9.413321
C	-1.390404	5.003049	13.440790
C	-1.446489	0.356523	12.602033
C	-3.388916	-1.076357	12.821683
H	-0.369864	0.486148	12.735947
H	-1.370311	-1.687169	13.305579
H	-3.834932	-2.040325	13.082578
H	-5.275000	-0.154281	12.295005
H	-4.272466	2.017997	11.721039
H	2.716802	11.437843	13.147614
H	3.404337	13.293474	14.604227
H	1.984126	13.968434	16.547948
H	-0.126444	12.710025	17.014018
H	-0.806783	10.848316	15.565639
H	-2.487334	6.745785	15.970198
H	-0.738690	6.448733	16.197412
H	-1.320936	7.291159	14.731525
H	-0.037881	0.940329	10.398412
H	1.536697	4.607301	13.789685
H	2.944269	4.795257	14.884971
H	1.301200	4.592148	15.564638
H	-4.237708	10.375831	12.918294
H	1.898607	11.265916	9.062867
H	2.619096	6.970274	16.602872
H	-2.519160	2.100719	14.484518
H	1.857965	9.514135	15.855375
H	-2.721971	7.327823	9.427367
H	-2.764302	6.590723	7.802256
H	-4.282194	6.794976	8.732861
H	-3.103072	2.007307	9.566594
H	2.587248	1.689527	9.919375
H	0.911532	11.906425	11.572315
H	-3.974600	4.040121	7.898334
H	-3.516578	6.809095	11.737481
H	-4.635561	7.479828	12.962069
H	-4.619378	8.156838	11.306577
H	-2.481524	4.083073	16.408069
H	-1.815053	11.491234	13.652424
H	2.486620	7.498896	9.010815
H	1.728695	8.642840	7.871340
H	3.361895	8.981740	8.521346
H	3.070402	5.105436	11.607974
H	4.032379	3.629683	11.303556

H	3.350311	4.555248	9.927693

2) $Ce(C3)_2bipy$

Ce	18.374770	7.254596	7.934107
N	20.186990	8.739720	5.229502
N	15.389096	5.737608	8.919556
N	21.479183	6.741312	6.177142
N	15.479513	5.852386	6.350140
N	20.157049	6.644735	9.893331
N	20.735290	9.771288	9.372912
N	21.369527	8.884881	7.508325
N	15.711895	9.864616	7.878652
N	20.800344	4.732445	6.597691
N	16.768667	4.914580	10.362014
N	17.006875	5.523425	4.855202
N	17.755636	7.916732	10.473349
N	14.822381	7.897541	7.753805
N	18.145500	8.984663	4.560843
C	20.227346	9.397922	4.006479
H	21.149551	9.707251	3.527950
C	19.933913	7.109836	11.182332
C	18.893492	8.485636	5.584863
C	20.392849	6.030615	6.586178
C	16.678101	5.309712	9.059911
C	18.944840	9.551785	3.581966
H	18.536232	10.009942	2.684255
C	18.662190	7.689341	11.498736
C	13.170350	5.829471	7.491705
C	21.336346	6.055287	9.635153
H	21.474335	5.694717	8.618731
C	20.263195	9.342643	8.167248
C	22.758006	8.885609	5.261402
C	16.811980	6.026688	6.106324
C	23.338272	10.124504	5.591203
H	22.966288	10.682224	6.453848
C	15.586099	5.127468	11.041390
H	15.459246	4.885793	12.094147
C	22.559297	5.894301	5.992311
H	23.543102	6.243434	5.696887
C	19.940162	10.464115	10.369545
H	20.124199	11.550276	10.322281
H	20.192761	10.105135	11.376027
H	18.879551	10.269949	10.178874
C	18.303359	8.035935	12.840382
H	19.000138	7.840199	13.654872
C	22.486131	8.976405	8.323824
H	23.471168	8.641583	8.012084
C	14.722826	5.660742	10.132303
H	13.692573	5.979782	10.259645
C	16.009517	8.557594	7.647069
C	23.254871	8.248937	4.105696
H	22.806203	7.310685	3.769568
C	20.973644	6.996201	12.159469
H	20.824229	7.404292	13.158819
C	24.376819	10.683250	4.837412
H	24.802426	11.648090	5.128799
C	22.365095	5.875778	10.549276
H	23.290085	5.381692	10.247176
C	22.170466	6.387348	11.856741
H	22.956789	6.311148	12.613173
C	22.093194	9.550551	9.495245
H	22.655275	9.814979	10.387756
C	17.079046	8.596014	13.126178
H	16.817470	8.851089	14.157125
C	16.679803	10.946154	7.872829
H	16.649451	11.491243	8.828716
H	16.466902	11.654615	7.056607
H	17.684510	10.528464	7.732440
C	16.561443	8.443231	10.791605
H	15.866919	8.578481	9.965877
C	24.293125	8.793220	3.343835
H	24.650519	8.265282	2.454773
C	16.161882	8.814685	12.067524
H	15.170141	9.239051	12.232565
C	17.943318	4.315293	10.966631
H	17.785835	3.237326	11.134677
H	18.162806	4.795309	11.930522
H	18.799462	4.457602	10.298412
C	13.815999	8.784406	8.100332
H	12.790297	8.478154	8.277046
C	14.870919	5.238597	5.262218
H	13.814962	4.995715	5.231290
C	12.743632	4.597536	8.021646
H	13.436755	3.995733	8.614382
C	24.865922	10.014893	3.711877
H	25.678859	10.445922	3.120610
C	14.369399	10.029446	8.167590
H	13.929855	10.998831	8.391009
C	15.828746	5.030331	4.320031
H	15.776650	4.579695	3.331655
C	22.134238	4.622849	6.245618
H	22.656132	3.669732	6.202918
C	10.542576	4.828357	7.033086
H	9.531199	4.447859	6.864023

C	16.698615	8.936024	4.451729
H	16.295963	8.423973	5.329742
H	16.401320	8.392512	3.541475
H	16.281384	9.954372	4.402117
C	12.239442	6.524468	6.693497
H	12.532460	7.460049	6.210638
C	18.263375	5.501783	4.128868
H	19.011160	6.054997	4.703950
H	18.138027	5.971244	3.141053
H	18.610702	4.466370	3.982705
C	11.452953	4.101781	7.805241
H	11.159677	3.141307	8.239290
C	10.945791	6.043029	6.469484
H	10.251903	6.615208	5.846565
C	19.971175	3.614370	7.008060
H	20.330431	3.190698	7.959495
H	19.986594	2.823508	6.242736
H	18.939883	3.964042	7.138587
B	21.453140	8.313694	6.046792
B	14.712425	6.327485	7.630910

3) Ce(Tp*)$_2$bipy

Ce	1.940604	12.327705	13.486625
N	3.770342	15.246251	13.762203
N	2.496698	14.805093	13.948885
N	5.083809	13.054095	14.090976
N	4.521406	11.841568	13.807692
N	4.570396	13.909592	11.755951
N	3.417354	13.265674	11.412849
N	-1.156359	11.289718	13.370359
N	-0.590100	12.194517	14.224711
N	-0.825929	12.838949	11.383041
N	0.286248	13.549912	11.730900
N	0.088683	10.473565	11.258824
N	1.388660	10.638739	11.627949
N	2.515490	12.351764	16.052640
N	1.513830	10.096497	14.809241
C	3.854280	16.564668	14.075390
C	2.588180	16.978321	14.485569
H	2.300879	17.977942	14.805318
C	1.767986	15.838659	14.387679
C	5.108468	17.368755	13.967906
H	5.911875	16.959122	14.599705
H	4.913457	18.401827	14.289301
H	5.488095	17.399183	12.934286
C	0.311428	15.712818	14.697713
H	-0.086466	14.736050	14.392641
H	-0.266730	16.495197	14.180061
H	0.124943	15.836303	15.777121
C	5.953502	12.935746	15.126633
C	5.971335	11.597869	15.508963
H	6.564764	11.153635	16.305451
C	5.064106	10.950054	14.650095
C	6.701714	14.090878	15.702131
H	7.375418	14.553416	14.962918
H	7.307529	13.755663	16.555766
H	6.017172	14.876756	16.058981
C	4.740078	9.492200	14.589678
H	3.790067	9.314721	14.073860
H	4.671248	9.061727	15.599683
H	5.531495	8.941312	14.052486
C	5.285950	14.232118	10.646590
C	4.563029	13.785338	9.547846
H	4.839152	13.882048	8.499573
C	3.396443	13.191994	10.074072
C	6.599029	14.945171	10.671892
H	6.508071	15.964965	11.079617
H	6.993829	15.024753	9.648725
H	7.343940	14.414019	11.285285
C	2.281787	12.597379	9.272302
H	2.598154	11.661974	8.783256
H	1.984230	13.292866	8.470945
H	1.406590	12.383765	9.888109
C	-1.948965	10.429513	14.060007
C	-1.913183	10.806407	15.398625
H	-2.439329	10.332786	16.224829
C	-1.054230	11.919538	15.452543
C	-2.680380	9.296597	13.421981
H	-3.439596	9.648606	12.704899
H	-3.188847	8.700568	14.192935
H	-1.995053	8.631203	12.873967
C	-0.703765	12.747555	16.646447
H	-0.565150	12.115497	17.536194
H	-1.514353	13.461091	16.875119
H	0.216628	13.318337	16.482031
C	-1.593648	13.549004	10.514874
C	-0.952248	14.761432	10.296567
H	-1.287196	15.571724	9.651903
C	0.223988	14.716661	11.073839
C	-2.872134	13.050100	9.923772
H	-2.714431	12.153927	9.302305
H	-3.312247	13.830735	9.286702
H	-3.609555	12.784217	10.697605
C	1.272065	15.781885	11.138986
H	2.201448	15.409038	11.574485

H	0.931192	16.644394	11.734291
H	1.485551	16.156803	10.125119
C	-0.004639	9.491677	10.325277
C	1.282223	9.008137	10.096764
H	1.567646	8.217839	9.405453
C	2.124990	9.761289	10.935584
C	-1.286635	9.061549	9.690517
H	-2.012787	8.704558	10.437023
H	-1.091504	8.242492	8.983810
H	-1.764271	9.884540	9.135592
C	3.609804	9.670201	11.081795
H	4.002455	10.450628	11.746246
H	4.103224	9.774039	10.101764
H	3.906220	8.689855	11.488968
C	3.072349	13.421011	16.653847
H	3.194471	14.304373	16.030820
C	3.483062	13.467740	17.975595
H	3.924962	14.379274	18.381424
C	3.314063	12.296206	18.757331
H	3.630215	12.268930	19.803702
C	2.750998	11.184899	18.173851
H	2.633293	10.277062	18.764361
C	2.340786	11.198535	16.804853
C	1.754095	10.052448	16.175501
C	1.412574	8.875134	16.910774
H	1.577249	8.841761	17.987240
C	0.859608	7.782551	16.283794
H	0.597136	6.890764	16.859532
C	0.631348	7.839480	14.884946
H	0.196846	7.004956	14.332156
C	0.970360	9.010024	14.227113
H	0.797470	9.080900	13.155664
B	4.884905	14.316692	13.205756
H	5.910866	14.945256	13.214358
B	-1.044685	11.380184	11.821494
H	-2.079573	10.984475	11.353246

4) $[Yb(C3)_2]I$

Yb	7.007603	12.383248	24.784614
N	8.482610	15.140315	25.858027
N	6.550280	15.215096	26.842365
N	9.201746	14.554692	23.446591
N	8.081705	13.834111	21.736461
N	10.193021	13.262541	25.339886
N	10.181359	11.125740	25.693258
N	5.031047	9.739179	24.986213
N	5.672778	9.998047	27.042964
N	4.281126	11.368025	23.122056
N	4.176700	13.530410	23.045660
N	6.231019	9.865507	22.696809
N	8.262561	10.370339	22.140652
C	7.317993	14.454592	26.023636
C	8.083644	13.855762	23.094480
C	9.365123	12.207912	25.586769
C	5.793822	10.523041	25.798271
C	4.775659	12.499799	23.698371
C	7.328025	10.562689	23.109665
C	8.425180	16.323140	26.581872
H	9.236979	17.041081	26.608549
C	7.212398	16.373911	27.201919
H	6.773287	17.122182	27.857474
C	5.206728	14.872310	27.277483
H	5.164490	14.796595	28.374823
H	4.922246	13.905867	26.841854
H	4.488493	15.637796	26.946748
C	9.905578	14.912372	22.309865
H	10.852339	15.440938	22.340606
C	9.194021	14.476649	21.230185
H	9.378924	14.573182	20.163052
C	7.047496	13.237978	20.904313
H	6.388560	12.626778	21.528696
H	7.504645	12.602042	20.133050
H	6.449540	14.021767	20.414686
C	11.500727	12.819315	25.244042
H	12.332608	13.478554	25.018098
C	11.500464	11.475475	25.480994
H	12.313789	10.754746	25.523491
C	9.731895	9.769706	25.958496
H	10.219846	9.375064	26.862644
H	9.970107	9.109754	25.110323
H	8.646181	9.777233	26.114153
C	10.842535	15.834973	25.130474
C	11.759607	15.761111	26.197270
H	11.766635	14.882828	26.847508
C	12.656193	16.796779	26.479078
H	13.353793	16.699317	27.316018
C	12.653905	17.957656	25.700345
H	13.353347	18.770333	25.915491
C	11.734298	18.073150	24.653971
H	11.702792	18.984070	24.049308
C	10.843081	17.029532	24.383840
H	10.113557	17.172083	23.583451
C	4.442585	8.733334	25.739972
H	3.784564	7.983289	25.316091

C	4.843346	8.891855	27.032830
H	4.610494	8.323638	27.930270
C	6.328115	10.513319	28.233297
H	5.583669	10.737341	29.012227
H	6.865599	11.436779	27.981780
H	7.045512	9.778527	28.630074
C	3.425608	11.706423	22.087302
H	2.944845	10.969556	21.452261
C	3.343801	13.068485	22.046736
H	2.785097	13.735809	21.395059
C	4.361731	14.935616	23.370042
H	4.484187	15.521467	22.447570
H	5.256276	15.046300	23.995342
H	3.489264	15.321510	23.920625
C	6.474516	9.297062	21.458853
H	5.728969	8.730071	20.911596
C	7.758703	9.598212	21.112038
H	8.345681	9.331949	20.236292
C	9.617487	10.896361	22.161440
H	10.345563	10.081155	22.292853
H	9.718667	11.603678	22.990109
H	9.837305	11.416578	21.218310
C	3.824559	8.745826	22.947885
C	4.299350	7.450011	22.662838
H	5.373744	7.251030	22.673082
C	3.434930	6.384822	22.391984
H	3.844447	5.394550	22.172419
C	2.051138	6.582812	22.411397
H	1.370118	5.754296	22.197548
C	1.549476	7.849686	22.722587
H	0.469202	8.016797	22.762573
C	2.426201	8.905959	22.992408
H	1.998181	9.873665	23.263767
B	9.695950	14.707814	24.938654
B	4.829891	9.921729	23.425583
I	4.534695	16.156260	19.314176

5) [Yb(Tp*)$_2$]I

Yb	0.117627	0.063942	0.190567
N	1.303187	1.557786	-1.147480
N	2.143031	-0.064383	1.300396
N	2.581352	1.218900	-1.490797
N	3.270752	-0.177453	0.536280
B	3.225977	-0.108748	-1.014286
C	2.508552	-0.175425	2.590517
C	3.894421	-0.372445	2.658139
C	4.345046	-0.365743	1.336643
C	3.114052	2.183505	-2.276628
C	1.026894	2.743908	-1.717898
C	2.146588	3.175695	-2.443449
C	5.740919	-0.500966	0.828549
C	1.521617	-0.049249	3.705630
C	-0.311532	3.395584	-1.582575
C	4.506620	2.142878	-2.810021
H	4.342978	-0.173712	-1.439261
H	4.502830	-0.489960	3.551839
H	2.253483	4.098651	-3.008831
H	5.841436	-1.335395	0.117282
H	6.064418	0.418891	0.316268
H	0.511638	-0.361065	3.401000
H	1.458084	0.995560	4.053189
H	-0.886130	2.982924	-0.741801
H	-0.202983	4.479887	-1.429672
H	-0.909106	3.252510	-2.498672
H	4.684010	1.248028	-3.426857
H	4.689361	3.030937	-3.430948
H	5.245150	2.140785	-1.993117
N	-1.118096	-1.527831	1.392028
N	-1.157867	1.509398	1.520405
N	1.117967	-1.547202	-1.190719
N	-1.802246	0.094338	-1.147697
N	2.411041	-1.315214	-1.568602
H	6.424126	-0.680566	1.670250
H	1.828353	-0.662439	4.565555
N	-2.461271	-1.318199	1.525400
C	-0.839018	-2.735086	1.913513
N	-2.478426	1.216975	1.709151
C	-0.885521	2.635517	2.203214
C	0.693876	-2.644456	-1.843385
N	-3.014127	0.105211	-0.513773
C	-2.032792	0.185162	-2.469945
C	2.804255	-2.253117	-2.460892
B	-3.138182	-0.010549	1.031982
C	-3.035172	-2.388425	2.124217
C	-2.025909	-3.316145	2.387876
C	0.553332	-3.276875	1.961517
C	-3.043856	2.150599	2.510877
C	-2.053194	3.073641	2.848665
C	0.469326	3.262694	2.178536
C	1.729894	-3.121993	-2.661167
C	-0.670847	-3.221562	-1.645100
C	-4.007570	0.213463	-1.427403
C	-3.416703	0.268535	-2.690097
C	-0.936605	0.139859	-3.484818
C	4.160805	-2.286376	-3.083799

H	-4.299530	-0.041040	1.323408
C	-4.496281	-2.489131	2.414645
H	-2.142853	-4.287796	2.862792
H	1.160262	-2.917269	1.118526
H	0.540028	-4.376226	1.936822
H	1.062424	-2.972701	2.891229
C	-4.479217	2.128499	2.921233
H	-2.168204	3.950374	3.482290
H	1.249271	2.552468	1.873087
H	0.500241	4.107164	1.470177
H	0.737809	3.661162	3.168035
H	1.707318	-3.988852	-3.318055
H	-1.406368	-2.453125	-1.373125
H	-0.665324	-3.976731	-0.841298
H	-1.011683	-3.722003	-2.563456
C	-5.457481	0.263562	-1.074142
H	-3.929138	0.357673	-3.645545
H	0.029814	0.442242	-3.062331
H	-0.821558	-0.881516	-3.885222
H	-1.169192	0.799330	-4.334179
H	4.371021	-1.365413	-3.650138
H	4.228878	-3.137255	-3.776045
H	4.954238	-2.394515	-2.327589
H	-4.832424	-1.690596	3.094856
H	-4.713304	-3.456220	2.889324
H	-5.099540	-2.414188	1.496157
H	-4.730644	1.208556	3.472480
H	-4.690587	2.987177	3.573656
H	-5.153038	2.185322	2.051722
H	-5.685855	1.113303	-0.411780
H	-5.783028	-0.652967	-0.557219
H	-6.057016	0.371891	-1.988794
I	4.377013	3.583633	1.176014

References

1. K. Izod, S. T. Liddle and W. Clegg, *Inorganic Chemistry*, 2004, **43**, 214-218.
2. T. V. Le and O. Daugulis, *Chemical Communications*, 2022, **58**, 537-540.
3. D. Savoia, C. Trombini and A. Umani-Ronchi, *Pure Appl. Chem.*, 1985, **57**, 1887-1896.
4. A. P. Forshaw, R. P. Bontchev and J. M. Smith, *Inorg. Chem.*, 2007, **46**, 3792-3794.
5. O. V. Dolomanov, L. J. Bourhis, R. J. Gildea, J. A. K. Howard and H. Puschmann, *J. Appl. Crystallogr.*, 2009, **42**, 339-341.
6. G. M. Sheldrick, *Acta Crystallogr., Sect. A:*, 2015, **71**, 3-8.
7. R. C. Clark and J. S. Reid, *Acta Crystallogr., Sect. A:*, 1995, **51**, 887-897.
8. T. Nishiura, A. Takabatake, M. Okutsu, J. Nakazawa and S. Hikichi, *Dalton Trans*, 2019, **48**, 2564-2568.
9. L. Falivene, R. Credendino, A. Poater, A. Petta, L. Serra, R. Oliva, V. Scarano and L. Cavallo, *Organometallics*, 2016, **35**, 2286-2293.
10. G. H. Maunder, A. Sella and D. A. Tocher, *Journal of the Chemical Society, Chemical Communications*, 1994, DOI: 10.1039/c39940000885, 885.
11. C. Lee, W. Yang and R. G. Parr, *Phys. Rev. B*, 1988, **37**, 785-789.
12. A. D. Becke, *Phys. Rev. A*, 1988, **38**, 3098-3100.
13. A. D. Becke, *J. Chem. Phys.*, 1993, **98**, 5648-5652.
14. E. Caldeweyher, S. Ehlert, A. Hansen, H. Neugebauer, S. Spicher, C. Bannwarth and S. Grimme, *J. Chem. Phys.*, 2019, **150**, 154122.
15. E. Caldeweyher, C. Bannwarth and S. Grimme, *J. Chem. Phys.*, 2017, **147**, 034112.
16. F. Neese, *WIREs Computational Molecular Science*, 2022, **12**, e1606.
17. A. V. Marenich, C. J. Cramer and D. G. Truhlar, *The Journal of Physical Chemistry B*, 2009, **113**, 6378-6396.
18. F. Weigend, *Phys. Chem. Chem. Phys.*, 2006, **8**, 1057-1065.
19. F. Weigend and R. Ahlrichs, *Phys. Chem. Chem. Phys.*, 2005, **7**, 3297-3305.

20. M. Dolg, H. Stoll and H. Preuss, *J. Chem. Phys.*, 1989, **90**, 1730-1734.
21. R. F. W. Bader, *Acc. Chem. Res.*, 1985, **18**, 9-15.
22. T. Lu and F. Chen, *J. Comput. Chem.*, 2012, **33**, 580-592.
23. E. D. Glendening, C. R. Landis and F. Weinhold, *J. Comput. Chem.*, 2019, **40**, 2234-2241.

Tris(carbene)borates; a new alternative for cyclopentadienide in organolanthanide chemistry

Authors:

Amy Price, Ankur Gupta, Wibe de Jong, Polly Arnold

Assoc Editor: Marinella Mazzanti

Dear Marinella,

We would like you to consider our manuscript as a communication in Chem Commun.

F block organometallic chemistry is now fifty years old, yet the carbon-based ligands used to support f-block chemistry are dominated by the cyclopentadienyl (**Cp**) anion and its derivatives, $[C_5H_nR_{5-n}]^-$ (n = 1-5; R = H, Me, tBu, Ph, SiMe3). The large cation size, fast ligand exchange kinetics, and low maximum formal oxidation state make it difficult to find new supporting organometallic ligands to manipulate the electronic structure and reactivity of lanthanide complexes. Meanwhile, lanthanide cyclopentadienyl complexes have shown some exciting properties, including single molecule magnetism, molecular qubit properties, reductive activation of small molecules, and photocatalytic C-F bond functionalizations. Further, recent redox reaction studies on organometallic lanthanide complexes have shown that different ligand sets yield different d or f-orbital occupations. Such ligand field effects were previously only considered applicable to d-block chemistry. Thus, there are many reasons to seek robust alternatives to these C_5, XL_2, ligands.

N-heterocyclic carbenes have seen application as σ-donating ligands to metals across the periodic table, and are highly tunable.[1-4] Yet ligands which coordinate through multiple carbenes have only rarely been used to bind f-block cations.[5-7] Trofimenko's tris(pyrazolyl)borate ligand, $[RB(N_2CRCHCR)_3]^-$ (**Tp**), has been widely used to support spectroscopically interesting lanthanide complexes, but like Cp, certain functionalized derivatives can be difficult to make. It also has a tendency to fall apart via B-N bond cleavage during subsequent reactions, and was originally referred to as a 'scorpionate' ligand because one arm of the chelate has a tendency to lift away from the body of the complex.

Here, we have used a monoanionic, tris(3-alkyl-imidazoline-2-yliden-1-yl)borate anion, **C3**, for the first time in f-block chemistry. This is the C-isomer of Tp, a true organometallic ligand. As a strong sigma-donor, it has the capacity to generate lanthanide complexes with new and different electronic structures to those of Cp. We show that while the steric profile is almost identical, it is a stronger donor, slightly more covalent, and that the two different ligands generate different f-orbital occupation for the Yb complexes – a feature of current great interest in the controlled design of molecular qubits.

Therefore, we hope you will consider that communication is of interest to the wide Chem Comm readership.

Best,

Polly et al

Chelating Ligands for f-block complexes